

# Optical properties of a two-nanospheroid cluster: analytical approach

D.V. Guzatov<sup>1,\*</sup> and V.V. Klimov<sup>2,†</sup>

<sup>1</sup>*Yanka Kupala Grodno State University,  
Ozheshko str. 22, 230023 Grodno, Belarus*

<sup>2</sup>*P.N. Lebedev Physical Institute, Russian Academy of Sciences,  
Leninsky pr. 53, 119991 Moscow, Russia*

(Dated: December 8, 2021)

## Abstract

Optical properties of a plasmonic nano-antenna made of two metallic nanospheroids (prolate or oblate) are investigated analytically in quasistatic approximation. It is shown that in clusters of two nanospheroids, three types of plasmonic modes can be present. Two of them can be effectively excited by a plane electromagnetic wave, while the third one can be effectively excited only by a nanolocalized light source (an atom, a molecule, a quantum dot) placed in the gap between the nanoparticles. Analytical expressions for absorption and scattering cross-sections, enhancement of a local field, and radiative decay rate of a dipole source placed near such a nano-antenna are presented and analyzed.

PACS numbers: 73.20.Mf, 78.67.-n

## I. INTRODUCTION

Nowadays, quite a number of works are devoted to the study of optical properties of single nanoparticles and their clusters. Special attention is paid to metal nanoparticles with the help of which it is possible to enhance electric fields at the frequencies of localized plasmon resonances<sup>1-3</sup>. On the basis of this effect, a variety of possible applications are considered. The most developed is use of large local fields near a rough surface for increasing of surface-enhanced Raman scattering (SERS)<sup>4</sup>. Modification of fluorescence by means of nanoparticles of different shapes is a basis for creation of nanobiosensors<sup>5-9</sup>, nano-antennas<sup>10-14</sup>, devices for decoding of DNA structure<sup>15</sup>, and etc.

At the present time, optical properties of single metallic nanospheres and their clusters<sup>16-29</sup>, single nanospheroids<sup>30-32</sup>, nanoellipsoids<sup>33-36</sup>, and some other nanobodies<sup>2,3,37</sup> are studied well enough from analytical point of view. Many other nanoparticles' shapes and also nanoparticles clusters are investigated only numerically. Unfortunately, numerical simulations often do not allow understanding of physical nature of interesting and complicated phenomena in this area. That is why any analytical solutions will have principal importance.

In this work, we present the results of an analytical study of optical properties of clusters of two metallic prolate or oblate spheroidal nanoparticles. Such clusters are investigated both experimentally and numerically and form a basis for various possible applications including nanosensors, nano-antennas, and plasmon waveguides<sup>38-44</sup>. As far as we know, there is no analytical investigation of optical properties of two-nanospheroid clusters. That is caused by extremely cumbersome mathematical calculations connected with use of general spheroidal wave functions and general rotational-translational addition theorems<sup>45-48</sup>. However, in the case of nanoparticles which sizes are less than the wavelength, i.e. in a quasistatic case, one can neglect retardation effects. It allows us to find an analytical solution for a cluster of two spheroidal nanoparticles, placed in an arbitrary external field. The geometry of the considered problem is shown in Fig. 1. For simplicity, we will consider that the cluster consists of two equal spheroids made of a material with dielectric constant  $\varepsilon$  and placed in vacuum. Generalization of our approach to unequal spheroids is straightforward and can be easily done with the help of the general theorem presented in the Appendix.

Main attention will be paid to a case of nearly touching and strongly interacting spheroids since it is the case that seems to be most interesting for applications because a substantial

enhancement of electric fields occurs there. The opposite case of weakly interacting spheroids can be easily treated with approximation of the spheroids by point dipoles with corresponding polarizabilities<sup>3</sup>.

For illustration of the analytical results obtained, we will consider a case of two identical (prolate or oblate) nanospheroids made of silver<sup>49</sup>. We suppose that the largest size of the nanospheroid is equal to 30 nm, and the aspect ratio of the spheroid is taken to be equal to 0.6.

The rest of the paper is organized as follows. In the Section II, free plasmon oscillations of a two-nanospheroid cluster are investigated. The results of this section reveal underlying physics and are necessary for interpretation of results of the other sections. In the Section III, we will consider optical properties of the two-nanospheroid cluster placed in the field of a plane electromagnetic wave. Here, we will find absorption and scattering cross-sections and the factor of local field enhancement also. In the Section IV, an object of examination is optical properties of the two-nanospheroid cluster placed in the field of a radiating atom or a molecule, and their decay rates will be calculated. In the Appendix, derivation of the translational addition theorem for spheroidal functions in a quasistatic case is presented. It is the theorem that allows one to find an analytical presentation of the solution for the two-nanospheroid cluster.

## II. PLASMON OSCILLATIONS IN A CLUSTER OF TWO NANOSPHEROIDS

It is well-known that all optical properties of nanoparticles can be derived from their plasmonic spectra, that is, from related plasmon eigenvalues  $\varepsilon_\nu$  and eigenfunctions  $\mathbf{e}_\nu$ ,  $\mathbf{h}_\nu$ , that are solution of the sourceless Maxwell equations<sup>50</sup>:

$$\begin{aligned} \text{roth}_\nu + i \left( \frac{\omega}{v_c} \right) \tilde{\varepsilon} \mathbf{e}_\nu &= 0, \\ \text{rote}_\nu - i \left( \frac{\omega}{v_c} \right) \mathbf{h}_\nu &= 0, \end{aligned} \tag{1}$$

where  $\tilde{\varepsilon} = \varepsilon_\nu$  inside the nanoparticle and  $\tilde{\varepsilon} = 1$  outside it,  $\omega$  is frequency of electromagnetic oscillations and  $v_c$  is the speed of light in vacuum. As a result, electric field in the presence of any nanoparticle can be presented in the following form<sup>50</sup>:

$$\mathbf{E}(\mathbf{r}) = \mathbf{E}_0(\mathbf{r}) + \sum_{\nu} \mathbf{e}_{\nu}(\mathbf{r}) \left( \frac{\varepsilon(\omega) - 1}{\varepsilon_{\nu} - \varepsilon(\omega)} \right) \frac{\int_V (\mathbf{e}_{\nu}(\mathbf{r}) \mathbf{E}_0(\mathbf{r})) dV}{\int_V (\mathbf{e}_{\nu}(\mathbf{r}) \mathbf{e}_{\nu}(\mathbf{r})) dV}, \quad (2)$$

where  $\varepsilon(\omega)$  describes the dependence of dielectric permittivity of nanoparticle's specific material on frequency  $\omega$ ,  $\mathbf{E}_0$  is the excitation field, and  $\nu$  is a vector index that defines specific plasmonic mode. From Eq. (2), it is possible to find any optical properties of a nanoparticle or a cluster of nanoparticles. So, to understand very complicated optical properties of a two-nanospheroid cluster, we should investigate plasmonic spectrum of this system at first.

For studying plasmon oscillations and other optical properties of clusters of two nanospheroids, it is enough to solve the quasistatic equations:

$$\operatorname{div}(\tilde{\varepsilon}\mathbf{e}_{\nu}) = 0, \quad \operatorname{rot}\mathbf{e}_{\nu} = 0, \quad (3)$$

that can be reduced to solution of Laplace equations by substituting  $\mathbf{e}_{\nu} = -\nabla\varphi_{\nu}$ :

$$\left. \begin{aligned} \Delta\varphi_{\nu}^{in} &= 0, & \text{inside the nanoparticle,} \\ \Delta\varphi_{\nu}^{out} &= 0, & \text{outside the nanoparticle,} \\ \varphi_{\nu}^{in}|_S &= \varphi_{\nu}^{out}|_S, \\ \varepsilon_{\nu} \frac{\partial\varphi_{\nu}^{in}}{\partial\mathbf{n}} \Big|_S &= \frac{\partial\varphi_{\nu}^{out}}{\partial\mathbf{n}} \Big|_S \end{aligned} \right\} \begin{array}{l} \text{at the surface} \\ \text{of the nanoparticle.} \end{array} \quad (4)$$

In Eq. (4),  $\varphi_{\nu}^{in}$ ,  $\varphi_{\nu}^{out}$  are the potentials of plasmonic eigenfunctions inside and outside the nanoparticle correspondingly, and  $\frac{\partial\varphi_{\nu}}{\partial\mathbf{n}} \Big|_S$  denotes normal derivative at the nanoparticles' surface  $S$ . The last equation in (4) provides continuity of normal components of electrical induction. Note that in this case there is no need to find magnetic fields for description of plasmonic oscillations.

The systems of equations obtained in such a way, have nontrivial solutions only for some negative values of permittivity  $\varepsilon_{\nu}$  defining frequency of plasmon oscillations<sup>2,3</sup>. In the case of Drude theory,  $\varepsilon(\omega) = 1 - \omega_{pl}^2/\omega^2$ , frequency of plasmon oscillations can be found from the expression

$$\omega_{\nu} = \frac{\omega_{pl}}{\sqrt{1 - \varepsilon_{\nu}}} < \omega_{pl}, \quad (5)$$

where  $\omega_{pl}$  is bulk plasmon frequency of a metal from which the nanoparticles are made. Our approach allows us to investigate arbitrary spheroids, but for simplicity in the present section we examine equations for plasmon oscillations in a cluster of two identical metal nanospheroids.

In our case of a two-nanospheroid cluster, we will look for a solution as follows. The total potential outside the spheroids will be the sum of their partial potentials (we will omit the mode index  $\nu$  further)<sup>19,51</sup>:

$$\varphi^{out} = \varphi_1^{out} + \varphi_2^{out}, \quad (6)$$

while the potentials inside each nanospheroid shall be denoted as  $\varphi_j^{in}$  ( $j = 1, 2$ ). To find  $\varphi^{out}$  and  $\varphi_1^{in}$ ,  $\varphi_2^{in}$ , it is naturally to use spheroidal coordinates. In the case of a prolate nanospheroid, the relation between Cartesian and spheroidal coordinates ( $1 \leq \xi < \infty$ ,  $-1 \leq \eta \leq 1$ ,  $0 \leq \phi \leq 2\pi$ ) is<sup>52</sup>:

$$\begin{aligned} x &= f \sqrt{(\xi^2 - 1)(1 - \eta^2)} \cos \phi, \\ y &= f \sqrt{(\xi^2 - 1)(1 - \eta^2)} \sin \phi, \\ z &= f \xi \eta, \end{aligned} \quad (7)$$

where  $f = \sqrt{c^2 - a^2}$  is a half of the focal distance in a prolate spheroid ( $a < c$ ) which surface is set by the equation  $(x^2 + y^2)/a^2 + z^2/c^2 = 1$ .

In the case of an oblate spheroid ( $a > c$ ), the relation between Cartesian and spheroidal coordinates ( $0 \leq \xi < \infty$ ,  $-1 \leq \eta \leq 1$ ,  $0 \leq \phi \leq 2\pi$ ) has the following form<sup>52</sup>:

$$\begin{aligned} x &= f \sqrt{(\xi^2 + 1)(1 - \eta^2)} \cos \phi, \\ y &= f \sqrt{(\xi^2 + 1)(1 - \eta^2)} \sin \phi, \\ z &= f \xi \eta, \end{aligned} \quad (8)$$

where  $f = \sqrt{a^2 - c^2}$  is a half of the focal distance in the oblate spheroid. Let us note that this expression can be obtained from Eq. (7) by substitution  $\xi \rightarrow i\xi$  and  $f \rightarrow -if$ . Further, we will use this formal replacement since it is fundamental and allows us to find a solution for oblate spheroids if the solution for prolate spheroid geometry is known<sup>51-54</sup>.

### A. Plasmon oscillations in a cluster of two identical prolate nanospheroids

To find plasmonic spectra of a two-nanospheroid cluster, it is naturally to use two local systems of spheroidal coordinates  $(\xi_j, \eta_j, \phi_j, j = 1, 2)$  the origins  $o_j$  of which are placed in the centers of corresponding nanospheroids (see Fig. 1(a)). Coordinates (and all other values) related to the first or second nanospheroid will be denoted by the index “1” or “2” respectively. The potential inside the  $j$ -th nanospheroid can be presented in the form<sup>55</sup> ( $j = 1, 2$ ):

$$\varphi_j^{in} = \sum_{n=0}^{\infty} \sum_{m=0}^n P_n^m(\xi_j) P_n^m(\eta_j) (A_{mn}^{(j)} \cos(m\phi_j) + B_{mn}^{(j)} \sin(m\phi_j)), \quad (9)$$

where  $P_n^m(\eta)$  is an associated Legendre function<sup>56</sup> defined in the region  $-1 \leq \eta \leq 1$ ,  $P_n^m(\xi)$  is an associated Legendre function<sup>56</sup> defined in a complex plane with the branch cut from  $-\infty$  to  $+1$ . The partial potential outside the  $j$ -th nanospheroid can be presented<sup>55</sup> as ( $j = 1, 2$ )

$$\varphi_j^{out} = \sum_{n=0}^{\infty} \sum_{m=0}^n Q_n^m(\xi_j) P_n^m(\eta_j) (C_{mn}^{(j)} \cos(m\phi_j) + D_{mn}^{(j)} \sin(m\phi_j)), \quad (10)$$

where  $Q_n^m(\xi)$  is an associated Legendre function of the second kind<sup>56</sup> defined in a complex plane with the branch cut from  $-\infty$  to  $+1$ .

By construction, the potentials (9) and (10) are solutions of the Laplace equation<sup>55</sup>. So to find a solution of Eq. (4), one should use only the boundary conditions:

$$\begin{aligned} \varphi_1^{in} \Big|_{\xi_1=\xi_0} &= \varphi_1^{out} \Big|_{\xi_1=\xi_0}, & \varepsilon \frac{\partial \varphi_1^{in}}{\partial \xi_1} \Big|_{\xi_1=\xi_0} &= \frac{\partial \varphi_1^{out}}{\partial \xi_1} \Big|_{\xi_1=\xi_0}, \\ \varphi_2^{in} \Big|_{\xi_2=\xi_0} &= \varphi_2^{out} \Big|_{\xi_2=\xi_0}, & \varepsilon \frac{\partial \varphi_2^{in}}{\partial \xi_2} \Big|_{\xi_2=\xi_0} &= \frac{\partial \varphi_2^{out}}{\partial \xi_2} \Big|_{\xi_2=\xi_0}, \end{aligned} \quad (11)$$

where  $\xi_0 = c/\sqrt{c^2 - a^2} = c/f$  are local radial coordinates defining surfaces of the nanospheroids,  $\varepsilon$  is permittivity of materials from which the nanoparticles are made. To reduce the boundary conditions (11) to a system of linear equations, we apply the translational addition theorem for wave functions of the prolate nanospheroid (see the Appendix). In the case of two identical coaxial nanospheroids, this theorem gives ( $j, s = 1, 2, j \neq s, \phi_1 = \phi_2$ )

$$Q_n^m(\xi_j) P_n^m(\eta_j) = \sum_{q=m}^{\infty} S_{mqmn}^{(j)} P_q^m(\xi_s) P_q^m(\eta_s), \quad (12)$$

where the functions  $S_{mqmn}^{(1)} = S_{mqmn}(f, f, l, 0)$  and  $S_{mqmn}^{(2)} = S_{mqmn}(f, f, l, \pi)$  are defined in the Appendix. Applying the boundary conditions (11) and the theorem (12), one can obtain the following system of equations ( $n = 0, 1, 2, \dots$ ;  $m = 0, 1, 2, \dots, n$ ):

$$\begin{aligned} & \left( \varepsilon \frac{dP_n^m(\xi_0)}{d\xi_0} Q_n^m(\xi_0) - P_n^m(\xi_0) \frac{dQ_n^m(\xi_0)}{d\xi_0} \right) C_{mn}^{(1)} \\ & + (\varepsilon - 1) P_n^m(\xi_0) \frac{dP_n^m(\xi_0)}{d\xi_0} \sum_{q=m}^{\infty} S_{mnmq}^{(0)} (-1)^{m+q} C_{mq}^{(2)} = 0, \\ & \left( \varepsilon \frac{dP_n^m(\xi_0)}{d\xi_0} Q_n^m(\xi_0) - P_n^m(\xi_0) \frac{dQ_n^m(\xi_0)}{d\xi_0} \right) (-1)^{m+n} C_{mn}^{(2)} \\ & + (\varepsilon - 1) P_n^m(\xi_0) \frac{dP_n^m(\xi_0)}{d\xi_0} \sum_{q=m}^{\infty} S_{mnmq}^{(0)} C_{mq}^{(1)} = 0. \end{aligned} \quad (13)$$

When deriving Eq. (13), we make use of the fact that for identical nanospheroids  $S_{mnmq}^{(2)} = (-1)^{n+q} S_{mnmq}^{(1)}$  (see the Appendix) and take  $S_{mnmq}^{(0)} = (-1)^{m+n} S_{mnmq}^{(1)}$ . The system of equations for  $D_{mn}^{(j)}$  is identical to (13) and gives no additional information for plasmonic spectra of coaxial spheroids. So, we will not consider it further.

As it results from symmetry of the considered cluster and the system (13), there are two independent types of solutions (plasmonic modes) with opposite parity. To select the first type of the modes (symmetric in  $z \rightarrow -z$  transformation), one should choose  $C_{mn}^{(1)} = (-1)^{m+n} C_{mn}^{(2)}$  in Eq. (13). As a result, we shall obtain the following system of equations for the symmetric modes:

$$\begin{aligned} & \left( \varepsilon \frac{dP_n^m(\xi_0)}{d\xi_0} Q_n^m(\xi_0) - P_n^m(\xi_0) \frac{dQ_n^m(\xi_0)}{d\xi_0} \right) C_{mn}^{(1)} \\ & + (\varepsilon - 1) P_n^m(\xi_0) \frac{dP_n^m(\xi_0)}{d\xi_0} \sum_{q=m}^{\infty} S_{mnmq}^{(0)} C_{mq}^{(1)} = 0. \end{aligned} \quad (14)$$

To obtain the second type of the modes (antisymmetric in  $z \rightarrow -z$  transformation), one should put  $C_{mn}^{(1)} = -(-1)^{m+n} C_{mn}^{(2)}$  in Eq. (13). As a result, we shall obtain the following system of equations for the antisymmetric modes:

$$\left( \varepsilon \frac{dP_n^m(\xi_0)}{d\xi_0} Q_n^m(\xi_0) - P_n^m(\xi_0) \frac{dQ_n^m(\xi_0)}{d\xi_0} \right) C_{mn}^{(1)} - (\varepsilon - 1) P_n^m(\xi_0) \frac{dP_n^m(\xi_0)}{d\xi_0} \sum_{q=m}^{\infty} S_{mnmq}^{(0)} C_{mq}^{(1)} = 0. \quad (15)$$

It is important to notice that separation of spectra into symmetric and antisymmetric plasmon modes is possible only in the case when there is a plane of symmetry. When  $m$  is even, antisymmetric modes have nonzero dipole moment and they are “bright” modes. On the contrary, symmetric modes have zero dipole moment and are “dark” modes when  $m$  is even. In the case of odd  $m$ , the “bright” and “dark” modes correspond to the symmetric and antisymmetric modes respectively. One can expect that the antisymmetric mode  $m = 0$  will have the largest polarizability and thus will be the “brightest” one for excitation of our cluster with a longitudinally (along the  $z$  axis) polarized plane wave.

To study plasmon oscillations in clusters of two prolate spheroidal nanoparticles, we have solved the eigenvalue problems (14) and (15) numerically. In Fig. 2, normalized plasmon frequency  $\omega/\omega_{pl}$  of a cluster of two prolate nanospheroids (see Fig. 1(a) for the geometry), corresponding to the first three plasmon modes, is shown as a function of normalized distances  $l/2c$  between the nanoparticles’ centers. Eigenvalues  $\varepsilon$  have been obtained as a nontrivial solution of the equations systems (14) and (15) in the case of an axis-symmetric problem ( $m = 0$ ). Then, the found solutions have been substituted into Eq. (5) to obtain plasmon oscillations frequency.

In Fig. 2, one can observe that plasmon frequencies of a cluster of two prolate nanospheroids tend to plasmon frequencies of a single nanospheroid (see Fig. 2(c)) if the distances between the nanospheroids are large enough. When width of the gap between the nanospheroids tends to zero, solutions of the equations (14) and (15) behave very differently. For symmetric modes (Fig. 2(a)), there are two branches: T-modes and M-modes. Modes of “T” type can be obtained by the method of hybridization of plasmon modes of a single prolate nanospheroid, analogously to the case of a cluster of two spherical nanoparticles<sup>25</sup>. When width of the gap between the nanoparticles is decreasing to zero, normalized plasmonic frequencies of T-modes tend to various values in the range from 0 to  $1/\sqrt{2}$ , on the analogy with a two-sphere cluster<sup>20,57</sup>. T-modes with higher indices (not shown for clarity) will concentrate near  $\omega/\omega_{pl} = 1/\sqrt{2}$ . In Fig. 2(a), one can also see that at very short distances

between the nanospheroids ( $l/2c < 1.1$ ), a new type of plasmonic modes (M-modes) appears. M-modes are characterized by strong spatial localization in the gap between the nanoparticles. As a result, they can be effectively excited only by a strongly nonuniform electric field of the molecule or the quantum dot. Values of plasmonic frequencies of these modes lie in the range  $\omega_{pl}/\sqrt{2} < \omega < \omega_{pl}$ . As the gap width decreases to zero, plasmon frequency of M-modes tends to bulk plasmon frequency  $\omega_{pl}$ .

In Fig. 2(b), nontrivial solutions of the equations system (15) for the antisymmetric potential in an axial-symmetric case ( $m = 0$ ), are shown. By analogy with a two-sphere cluster, we will call these modes L-modes (longitudinal) because they are "bright" only for longitudinal excitation. These modes can be described by the hybridization method of plasmon oscillations of single nanospheroids forming the considered cluster. As width of the gap between prolate nanospheroids decreases to zero, normalized plasmon frequencies of these modes tend to zero as it also takes place in the case of spherical nanoparticles<sup>20,57</sup>. Plasmonic frequencies of L-modes of higher orders (not shown) tend to  $\omega_{pl}/\sqrt{2}$ , and concentration of infinite number of L-modes occurs near this value.

In Fig. 3, distribution of a surface charge of plasmonic modes of the lowest order in clusters of two identical prolate nanospheroids, is shown. It is seen in this figure that the T- and M-modes have symmetric distribution of the surface charge in contrast to the antisymmetric L=1 mode. This behavior, of course, is in agreement with symmetry of the equations (14) and (15). Another interesting feature is that the surface charge of T-modes is distributed over the surface of the all nanoparticles for any distances between them, while for M- and L-modes it is concentrated near the gap between the nanospheroids if the distance between them is sufficiently small. It is interesting to note also that the surface charge of M-modes is more concentrated in comparison with that of L-modes. Indeed, due to an electroneutrality requirement, the total surface charge on each nanospheroid should be equal to zero. Here, both positive and negative charges of M-modes are localized near the gap between the nanoparticles so that on the rest of nanoparticles the charge is almost equal to zero, as it is well seen in Fig. 3(a). At the same time, in the case of L-modes for each of nanospheroids near the gap a charge of only one sign is concentrated, and a charge of the opposite sign is distributed with small magnitude over the remaining surface of the nanoparticles. Therefore, strictly speaking, the surface charge in an L-mode is distributed over the whole surface of the cluster nanoparticles though it is not clearly seen at small

distances between the nanoparticles (see Fig. 3(a)). As the distance increases, the charge distribution changes in the cluster: it spreads over the nanoparticles' surface, tending in the limit to a distribution corresponding to single prolate nanospheroids (see Fig. 3(c)).

### B. Plasmon oscillations in a cluster of two identical oblate nanospheroids

In this geometry, one should also use local systems of coordinates  $(\xi_j, \eta_j, \phi_j, j = 1, 2)$  which are connected with each nanospheroid and have origins  $o_j$  in their centers (see Fig. 1(b)). Now, the electric potential inside the  $j$ -th nanospheroid can be presented in the form ( $j = 1, 2$ ):

$$\varphi_j^{in} = \sum_{n=0}^{\infty} \sum_{m=0}^n P_n^m(i\xi_j) P_n^m(\eta_j) (A_{mn}^{(j)} \cos(m\phi_j) + B_{mn}^{(j)} \sin(m\phi_j)), \quad (16)$$

and the partial potential outside the  $j$ -th oblate nanospheroid will look like ( $j = 1, 2$ ):

$$\varphi_j^{out} = \sum_{n=0}^{\infty} \sum_{m=0}^n Q_n^m(i\xi_j) P_n^m(\eta_j) (C_{mn}^{(j)} \cos(m\phi_j) + D_{mn}^{(j)} \sin(m\phi_j)). \quad (17)$$

The total potential outside the nanospheroids will be expressed by Eq. (6). As boundary conditions for the potential, Eq. (11), where  $\xi_0 = c/\sqrt{a^2 - c^2} = c/f$ , is used. In the case of oblate nanospheroids, the addition translation theorem (see the Appendix) has the following form ( $j, s = 1, 2, j \neq s$ ):

$$Q_n^m(i\xi_j) P_n^m(\eta_j) \begin{cases} \cos(m\phi_j) \\ \sin(m\phi_j) \end{cases} = \sum_{q=0}^{\infty} \sum_{p=0}^q P_q^p(i\xi_s) P_q^p(\eta_s) \begin{cases} M_{pqmn}^{(j)} \cos(p\phi_s) \\ N_{pqmn}^{(j)} \sin(p\phi_s) \end{cases}, \quad (18)$$

where the functions  $M_{pqmn}^{(1)} = M_{pqmn}(-if, -if, l, \pi)$ ,  $N_{pqmn}^{(1)} = N_{pqmn}(-if, -if, l, \pi)$  and  $M_{pqmn}^{(2)} = M_{pqmn}(-if, -if, l, 0)$ ,  $N_{pqmn}^{(2)} = N_{pqmn}(-if, -if, l, 0)$  are defined in the Appendix. Now, substituting Eqs. (16) and (17) into Eq. (11) and making use of the addition translation theorem (18), we shall obtain the following system of equations ( $n = 0, 1, 2, \dots; m = 0, 1, 2, \dots, n$ ):

$$\begin{aligned}
& \left( \varepsilon \frac{dP_n^m(i\xi_0)}{d\xi_0} Q_n^m(i\xi_0) - P_n^m(i\xi_0) \frac{dQ_n^m(i\xi_0)}{d\xi_0} \right) C_{mn}^{(1)} \\
& + (\varepsilon - 1) P_n^m(i\xi_0) \frac{dP_n^m(i\xi_0)}{d\xi_0} \sum_{q=0}^{\infty} \sum_{p=0}^q M_{mnpq}^{(0)} (-1)^p C_{pq}^{(2)} = 0, \\
& \left( \varepsilon \frac{dP_n^m(i\xi_0)}{d\xi_0} Q_n^m(i\xi_0) - P_n^m(i\xi_0) \frac{dQ_n^m(i\xi_0)}{d\xi_0} \right) (-1)^m C_{mn}^{(2)} \\
& + (\varepsilon - 1) P_n^m(i\xi_0) \frac{dP_n^m(i\xi_0)}{d\xi_0} \sum_{q=0}^{\infty} \sum_{p=0}^q M_{mnpq}^{(0)} C_{pq}^{(1)} = 0. \tag{19}
\end{aligned}$$

By deriving Eq. (19), we take into account that  $M_{mnpq}^{(2)} = (-1)^{m+p} M_{mnpq}^{(1)}$  (see the Appendix) and denote  $M_{mnpq}^{(0)} = (-1)^m M_{mnpq}^{(1)}$ . The system of equations for  $D_{mn}^{(j)}$  is analogous to Eq. (19), and we will not analyze it here.

Due to symmetry of a cluster of two identical oblate nanospheroids, there are two types of plasmon oscillation: symmetric and antisymmetric relatively the symmetry plane. To select the first (symmetric in  $x \rightarrow -x$  transformation) type, we take  $C_{mn}^{(1)} = (-1)^m C_{mn}^{(2)}$ . As a result, we shall obtain the system of equations:

$$\begin{aligned}
& \left( \varepsilon \frac{dP_n^m(i\xi_0)}{d\xi_0} Q_n^m(i\xi_0) - P_n^m(i\xi_0) \frac{dQ_n^m(i\xi_0)}{d\xi_0} \right) C_{mn}^{(1)} \\
& + (\varepsilon - 1) P_n^m(i\xi_0) \frac{dP_n^m(i\xi_0)}{d\xi_0} \sum_{q=0}^{\infty} \sum_{p=0}^q M_{mnpq}^{(0)} C_{pq}^{(1)} = 0. \tag{20}
\end{aligned}$$

To select the second (antisymmetric in  $x \rightarrow -x$  transformation) type of plasmon modes in Eq. (19), we take  $C_{mn}^{(1)} = -(-1)^m C_{mn}^{(2)}$ . As a result, we shall have

$$\begin{aligned}
& \left( \varepsilon \frac{dP_n^m(i\xi_0)}{d\xi_0} Q_n^m(i\xi_0) - P_n^m(i\xi_0) \frac{dQ_n^m(i\xi_0)}{d\xi_0} \right) C_{mn}^{(1)} \\
& - (\varepsilon - 1) P_n^m(i\xi_0) \frac{dP_n^m(i\xi_0)}{d\xi_0} \sum_{q=0}^{\infty} \sum_{p=0}^q M_{mnpq}^{(0)} C_{pq}^{(1)} = 0. \tag{21}
\end{aligned}$$

In Fig. 4, the dependence of normalized plasmon frequencies  $\omega/\omega_{pl} = 1/\sqrt{1-\varepsilon}$  of a cluster of two identical oblate nanospheroids on normalized distances  $l/2a$  between the nanoparticles' centers, is shown for the first three plasmon modes. Eigenvalues  $\varepsilon$  were obtained as a solution of the equations systems (20) and (21).

One can see in Fig. 4 that in clusters of two oblate nanospheroids, modes of “T”, “M”, and “L” types, that are analogous to T-, M- and L-modes of a cluster made of two prolate spheroids (see Fig. 2), can exist. The T- and M-modes are the solutions of the system (20), while the L-modes are the solution of the system (21). T- and L-modes can be derived by the method of hybridization of plasmonic modes of two oblate nanospheroids and their plasmonic frequencies are lying in the range  $0 < \omega < \omega_{pl}/\sqrt{2}$ . An infinite number of plasmonic frequencies of higher L-and T-modes lie near  $\omega_{pl}/\sqrt{2}$ . When width of the gap decreases to 0, the ratio  $\omega/\omega_{pl}$  for T-modes tends to various values in the range from 0 to  $1/\sqrt{2}$ , while plasmonic frequencies of L-modes approach zero by analogy with L-modes in a cluster of two spherical nanoparticles<sup>20,57</sup>. Plasmonic frequencies of strongly localized M-modes (Fig. 4(a)) lie in the range  $\omega_{pl}/\sqrt{2} < \omega < \omega_{pl}$ , as it happens in a cluster of two spherical nanoparticles<sup>20,57</sup>. As width of the gap between oblate nanospheroids decreases to zero, plasmon frequencies of M-modes tend to bulk plasmon frequency  $\omega_{pl}$  analogously to the case of a two-sphere cluster<sup>20,57</sup>. For large distances between the spheroids, M-modes disappear, and plasmon frequencies of L- and T-modes of a cluster of two oblate nanospheroids tend to plasmonic frequencies of a single spheroid (see. Fig. 4(c)) and can be found by means of a self-consistent model with approximation of spheroids by anisotropic point dipoles.

In Fig. 5, the distribution of a surface charge of plasmon modes of lower orders in a cluster of two identical oblate nanospheroids is shown. One can see in this figure that the charge distribution is symmetric in T- and M-modes, while in L-mode it is antisymmetric in agreement with the definition of these modes. For small distances between nanospheroids, charges in M- and L-modes are strongly localized near the gap. On the contrary, when the distance between the spheroids increases, the charge distribution tends to symmetric or antisymmetric combination of a surface charge in a single oblate nanospheroid (see Fig. 5(c)).

Thus, in a cluster of two oblate or prolate spheroidal nanoparticles, fundamental symmetric and antisymmetric plasmon modes of “T”, “M”, and “L” types can be excited, and it is these modes that define all optical properties of a two-nanospheroid cluster.

### III. A CLUSTER OF TWO METAL NANOSPHEROIDS IN THE FIELD OF A PLANE ELECTROMAGNETIC WAVE

In this section, we will consider a two-spheroid cluster in a uniform electric field with the potential

$$\varphi_0 = -E_{0x}x - E_{0y}y - E_{0z}z, \quad (22)$$

where the time factor  $e^{-i\omega t}$  is omitted. This case corresponds to a plane wave incidence and is important for transformation of far fields into near fields, for enhancement of electric fields, and for effective excitation of atoms and molecules. Here again, we restrict ourselves to two special cases of nanospheroids' shape and position which are most interesting for applications. In the first case, two prolate nanospheroids have a general axis of rotation  $z$ , and axes  $x$  and  $y$  are parallel (Fig. 1(a)). In the second case, two oblate nanospheroids have parallel axes of rotation  $z$  and general axis  $x$ , i.e., the centers of the nanoparticles are located in the plane that is perpendicular to the axes of rotation (Fig. 1(b)). The distance between the nanospheroids' centers is more than a half-sum of the lengths between their foci (the nanoparticles are not overlapping).

#### A. A cluster of two prolate nanospheroids

Here, we also will use local systems of spheroidal coordinates, the origins of which are placed in the nanospheroids' centers (see Fig. 1(a)). The potential inside the  $j$ -th nanospheroid again can be presented as a series in spheroidal harmonics (9), while the potential outside the nanospheroids now should be presented in the form:

$$\varphi^{out} = \varphi_1^{out} + \varphi_2^{out} + \varphi_0, \quad (23)$$

where  $\varphi_1^{out}$ ,  $\varphi_2^{out}$  are contributions from the first and second nanospheroids (see Eq. (10)), and  $\varphi_0$  is the potential of the external electric field (22).

Electric potential of the incident plane wave (22) in local coordinates of the  $j$ -th ( $j = 1, 2$ ) prolate nanospheroids, looks like:

$$\begin{aligned}\varphi_0^{(j)} = & f (E_{0x} \cos (\phi_j) + E_{0y} \sin (\phi_j)) P_1^1 (\xi_j) P_1^1 (\eta_j) \\ & - f E_{0z} P_1 (\xi_j) P_1 (\eta_j) + (-1)^{j+1} E_{0z} \frac{l}{2},\end{aligned}\quad (24)$$

To find electric potentials and electric fields inside and outside the spheroids, one should use the boundary conditions for the potential:

$$\begin{aligned}\varphi_1^{in} \Big|_{\xi_1=\xi_0} &= \left( \varphi_1^{out} + \varphi_2^{out} + \varphi_0^{(1)} \right) \Big|_{\xi_1=\xi_0}, \\ \varepsilon \frac{\partial \varphi_1^{in}}{\partial \xi_1} \Big|_{\xi_1=\xi_0} &= \frac{\partial \left( \varphi_1^{out} + \varphi_2^{out} + \varphi_0^{(1)} \right)}{\partial \xi_1} \Big|_{\xi_1=\xi_0}, \\ \varphi_2^{in} \Big|_{\xi_2=\xi_0} &= \left( \varphi_1^{out} + \varphi_2^{out} + \varphi_0^{(2)} \right) \Big|_{\xi_2=\xi_0}, \\ \varepsilon \frac{\partial \varphi_2^{in}}{\partial \xi_2} \Big|_{\xi_2=\xi_0} &= \frac{\partial \left( \varphi_1^{out} + \varphi_2^{out} + \varphi_0^{(2)} \right)}{\partial \xi_2} \Big|_{\xi_2=\xi_0},\end{aligned}\quad (25)$$

where  $\xi_0 = c/\sqrt{c^2 - a^2} = c/f$  is local radial coordinate that defines surfaces of the nanoparticles,  $\varepsilon$  is permittivity of the nanoparticle's material. Making use of the boundary conditions (25) and the addition translation theorem (12), one can obtain the following system of equations for the coefficients  $C_{mn}^{(1)}$ ,  $C_{mn}^{(2)}$ ,  $D_{mn}^{(1)}$  and  $D_{mn}^{(2)}$  that define the outside field (see Eq. (10) and Eq. (23)) ( $n = 0, 1, 2, \dots$ ;  $m = 0, 1, 2, \dots, n$ ):

$$\begin{aligned}& \left( \varepsilon \frac{dP_n^m(\xi_0)}{d\xi_0} Q_n^m(\xi_0) - P_n^m(\xi_0) \frac{dQ_n^m(\xi_0)}{d\xi_0} \right) C_{mn}^{(1)} \\ & + (\varepsilon - 1) P_n^m(\xi_0) \frac{dP_n^m(\xi_0)}{d\xi_0} \sum_{q=m}^{\infty} S_{mnmq}^{(2)} C_{mq}^{(2)} = a_{mn}^{(1)} (\varepsilon - 1) P_n^m(\xi_0) \frac{dP_n^m(\xi_0)}{d\xi_0}, \\ & \left( \varepsilon \frac{dP_n^m(\xi_0)}{d\xi_0} Q_n^m(\xi_0) - P_n^m(\xi_0) \frac{dQ_n^m(\xi_0)}{d\xi_{02}} \right) C_{mn}^{(2)} \\ & + (\varepsilon - 1) P_n^m(\xi_0) \frac{dP_n^m(\xi_0)}{d\xi_0} \sum_{q=m}^{\infty} S_{mnmq}^{(1)} C_{mq}^{(1)} = a_{mn}^{(2)} (\varepsilon - 1) P_n^m(\xi_0) \frac{dP_n^m(\xi_0)}{d\xi_0},\end{aligned}\quad (26)$$

and ( $n = 1, 2, 3, \dots$ ;  $m = 1, 2, 3, \dots, n$ )

$$\begin{aligned}
& \left( \varepsilon \frac{dP_n^m(\xi_0)}{d\xi_0} Q_n^m(\xi_0) - P_n^m(\xi_0) \frac{dQ_n^m(\xi_0)}{d\xi_0} \right) D_{mn}^{(1)} \\
& + (\varepsilon - 1) P_n^m(\xi_0) \frac{dP_n^m(\xi_0)}{d\xi_0} \sum_{q=m}^{\infty} S_{mnmq}^{(2)} D_{mq}^{(2)} = b_{mn}^{(1)} (\varepsilon - 1) P_n^m(\xi_0) \frac{dP_n^m(\xi_0)}{d\xi_0}, \\
& \left( \varepsilon \frac{dP_n^m(\xi_0)}{d\xi_0} Q_n^m(\xi_0) - P_n^m(\xi_0) \frac{dQ_n^m(\xi_0)}{d\xi_0} \right) D_{mn}^{(2)} \\
& + (\varepsilon - 1) P_n^m(\xi_0) \frac{dP_n^m(\xi_0)}{d\xi_0} \sum_{q=m}^{\infty} S_{mnmq}^{(1)} D_{mq}^{(1)} = b_{mn}^{(2)} (\varepsilon - 1) P_n^m(\xi_0) \frac{dP_n^m(\xi_0)}{d\xi_0},
\end{aligned} \tag{27}$$

where the coefficients

$$\begin{aligned}
a_{mn}^{(j)} &= -\delta_{n1} f (\delta_{m1} E_{0x} - \delta_{m0} E_{0z}) + (-1)^j \delta_{n0} \delta_{m0} E_{0z} \frac{l}{2}, \\
b_{mn}^{(1)} &= b_{mn}^{(2)} = -\delta_{m1} \delta_{n1} f E_{0y},
\end{aligned} \tag{28}$$

define excitation field. In Eq. (28),  $\delta_{n1}$  is Kronecker delta symbol. It should be noted here that due to axial symmetry of the considered cluster, the systems of equations (26) and (27) allow one to find the coefficients  $C_{mn}^{(j)}$  and  $D_{mn}^{(j)}$  for given order  $m$ , while degree  $n$  runs over  $n = m, m + 1, m + 2, \dots, m + N$ , where  $N$  is a large number that defines accuracy of the solution.

Induced dipole moment of a cluster of two prolate nanospheroids, placed in the field of a plane electromagnetic wave, can be calculated by analogy with a single prolate nanospheroid<sup>31</sup>, that is, by finding far field asymptotes of the potential (23). As a result, for dipole moment induced in the  $j$ -th nanospheroid ( $j = 1, 2$ ) we have

$$d_x^{(j)} = \frac{2f^2}{3} C_{11}^{(j)}, \quad d_y^{(j)} = \frac{2f^2}{3} D_{11}^{(j)}, \quad d_z^{(j)} = \frac{f^2}{3} C_{01}^{(j)}, \tag{29}$$

and the total dipole moment of the cluster will be the sum of the momenta (29). Scattering and absorption cross-sections can be easily found if the dipole momenta (29) are known<sup>58</sup>:

$$\sigma^{abs} = 4\pi \left( \frac{\omega}{v_c} \right) \frac{\text{Im}(\mathbf{d}\mathbf{E}_0^*)}{|\mathbf{E}_0|^2}, \quad \sigma^{scat} = \frac{8\pi}{3} \left( \frac{\omega}{v_c} \right)^4 \frac{|\mathbf{d}|^2}{|\mathbf{E}_0|^2}, \tag{30}$$

where  $\mathbf{d} = \mathbf{d}^{(1)} + \mathbf{d}^{(2)}$  denotes dipole momentum of the whole system, and asterix denotes an operation of the complex conjugation.

In Fig. 6, absorption (a) and scattering (b) cross-sections of a cluster of two identical prolate nanospheroids made from silver, are shown as a function of the wavelength. For longitudinal ( $z$ ) polarization, both of the cross-sections have two peaks that correspond to longitudinal plasmonic oscillations with  $L = 1, 2$  (see Fig. 2(b)). It is very important that both of the peaks are split substantially relatively the case of a single spheroid (the “ $z$ ” dashed curve) due to strong interaction between the nanospheroids.

On the contrary, for transversal ( $x$  or  $y$ ) polarization one can see only one peak due to excitation of the symmetrical  $T = 1$  mode, and this peak is shifted just slightly relatively the single spheroid resonance (the “ $y$ ” dashed curve). It means that transversal ( $x$  or  $y$  polarization) excitation of a two-spheroid cluster induces only weak interaction between the nanospheroids (see the dispersion curves for  $T$ -modes on Fig. 2(a)). Due to this weak interaction, absorption and scattering cross-sections are approximately equal to doubled and quadrupled cross-section of a single spheroid respectively.

It should be noticed that in Fig. 6 the maxima of absorption, corresponding to plasmon oscillations of  $M$ -type that should lie in the interval  $\omega_{pl}/\sqrt{2} < \omega < \omega_{pl}$ , that corresponds to  $326 < \lambda < 337$  nm for silver<sup>49</sup>, are not visible. It is related to the fact that  $M$ -modes interact with a homogeneous electric field weakly and can be effectively excited only by a source of radiation that is nonuniform in comparison with a size of the gap between the nanoparticles<sup>57</sup> (see Fig. 3).

To control correctness and accuracy of our analytical calculations, we have also carried out finite element simulation of this system with Comsol Multiphysics® software. The results of this simulation are shown by the circles in Fig. 6. One can see that there is a fine agreement between the analytical and pure numerical calculations. This fact confirms correctness and accuracy of the both of approaches.

## **B. A cluster of two oblate nanospheroids**

The case of two oblate nanospheroids is in many aspects similar to the case of two prolate nanospheroids, considered above. So let us again choose local systems of coordinates that are connected with each of the nanospheroids and have origins in their centers (see Fig. 1(b)). The potential inside the  $j$ -th nanospheroid again can be presented as a series in spheroidal harmonics (16), while the potential outside the oblate spheroids can be presented in the

form:

$$\varphi^{out} = \varphi_1^{out} + \varphi_2^{out} + \varphi_0, \quad (31)$$

where  $\varphi_1^{out}, \varphi_2^{out}$  are contributions from the first and second nanospheroids (see Eq. (17)) and  $\varphi_0$  is the potential of the external electric field (22). In the local coordinates of the  $j$ -th ( $j = 1, 2$ ) oblate nanospheroids, it looks like

$$\begin{aligned} \varphi_0^{(j)} = & -if (E_{0x} \cos(\phi_j) + E_{0y} \sin(\phi_j)) P_1^1(i\xi_j) P_1^1(\eta_j) \\ & + if E_{0z} P_1(i\xi_j) P_1(\eta_j) + (-1)^j E_{0x} \frac{l}{2}. \end{aligned} \quad (32)$$

Making use of the boundary conditions (25) with  $\xi_0 = c/\sqrt{a^2 - c^2} = c/f$  and the addition-translation theorem (18), we shall obtain the following systems of equations ( $n = 0, 1, 2, \dots; m = 0, 1, 2, \dots, n$ ):

$$\begin{aligned} & \left( \varepsilon \frac{dP_n^m(i\xi_0)}{d\xi_0} Q_n^m(i\xi_0) - P_n^m(i\xi_0) \frac{dQ_n^m(i\xi_0)}{d\xi_0} \right) C_{mn}^{(1)} \\ & + (\varepsilon - 1) P_n^m(i\xi_0) \frac{dP_n^m(i\xi_0)}{d\xi_0} \sum_{q=0}^{\infty} \sum_{p=0}^q M_{mnpq}^{(2)} C_{pq}^{(2)} = a_{mn}^{(1)} (\varepsilon - 1) P_n^m(i\xi_0) \frac{dP_n^m(i\xi_0)}{d\xi_0}, \\ & \left( \varepsilon \frac{dP_n^m(i\xi_0)}{d\xi_0} Q_n^m(i\xi_0) - P_n^m(i\xi_0) \frac{dQ_n^m(i\xi_0)}{d\xi_0} \right) C_{mn}^{(2)} \\ & + (\varepsilon - 1) P_n^m(i\xi_0) \frac{dP_n^m(i\xi_0)}{d\xi_0} \sum_{q=0}^{\infty} \sum_{p=0}^q M_{mnpq}^{(1)} C_{pq}^{(1)} = a_{mn}^{(2)} (\varepsilon - 1) P_n^m(i\xi_0) \frac{dP_n^m(i\xi_0)}{d\xi_0}, \end{aligned} \quad (33)$$

and ( $n = 1, 2, 3, \dots; m = 1, 2, 3, \dots, n$ )

$$\begin{aligned} & \left( \varepsilon \frac{dP_n^m(i\xi_0)}{d\xi_0} Q_n^m(i\xi_0) - P_n^m(i\xi_0) \frac{dQ_n^m(i\xi_0)}{d\xi_0} \right) D_{mn}^{(1)} \\ & + (\varepsilon - 1) P_n^m(i\xi_0) \frac{dP_n^m(i\xi_0)}{d\xi_0} \sum_{q=1}^{\infty} \sum_{p=1}^q N_{mnpq}^{(2)} D_{pq}^{(2)} = b_{mn}^{(1)} (\varepsilon - 1) P_n^m(i\xi_0) \frac{dP_n^m(i\xi_0)}{d\xi_0}, \\ & \left( \varepsilon \frac{dP_n^m(i\xi_0)}{d\xi_0} Q_n^m(i\xi_0) - P_n^m(i\xi_0) \frac{dQ_n^m(i\xi_0)}{d\xi_0} \right) D_{mn}^{(2)} \\ & + (\varepsilon - 1) P_n^m(i\xi_0) \frac{dP_n^m(i\xi_0)}{d\xi_0} \sum_{q=1}^{\infty} \sum_{p=1}^q N_{mnpq}^{(1)} D_{pq}^{(1)} = b_{mn}^{(2)} (\varepsilon - 1) P_n^m(i\xi_0) \frac{dP_n^m(i\xi_0)}{d\xi_0}, \end{aligned} \quad (34)$$

where

$$\begin{aligned} a_{mn}^{(j)} &= i\delta_{n1}f(\delta_{m1}E_{0x} - \delta_{m0}E_{0z}) + (-1)^{j+1}\delta_{m0}\delta_{n0}E_{0x}\frac{l}{2}, \\ b_{mn}^{(1)} &= b_{mn}^{(2)} = i\delta_{m1}\delta_{n1}fE_{0y}. \end{aligned} \quad (35)$$

Apparently, the equations (33) and (34) have more complicated structure than Eqs. (26) and (27) because now, due to lack of axial symmetry, one can not split the system of equations into systems with fixed order  $m$  of the Legendre function.

For calculation of absorption and scattering cross-sections of a cluster in the field of a plane electromagnetic wave, one can again use Eq. (30), where dipole momenta of each spheroid can be expressed through the solutions of Eqs. (33) and (34) ( $j = 1, 2$ )

$$d_x^{(j)} = -\frac{2f^2}{3}C_{11}^{(j)}, \quad d_y^{(j)} = -\frac{2f^2}{3}D_{11}^{(j)}, \quad d_z^{(j)} = -\frac{f^2}{3}C_{01}^{(j)}. \quad (36)$$

In Fig. 7, the absorption (a) and scattering (b) cross-sections of a cluster of two identical oblate nanospheroids made from silver are shown as a function of wavelength. For longitudinal (x) polarization, both the cross-sections have two peaks, that correspond to antisymmetric plasmonic oscillations with  $L = 1, 2$  (see Fig. 4(b)). It is very important that now only one peak ( $L = 1$ ) is shifted substantially relatively the case of a single spheroid (the “x, y” dashed curves) due to strong interaction between the nanospheroids. The  $L = 2$  mode suffers only a small shift in agreement with Fig. 4(b).

For transversal (y) polarization, one can see only one peak due to excitation of the symmetrical  $T = 1$  mode, and this peak is only slightly shifted relatively the single spheroid resonance (the dashed curve). It means that transversal (y polarization) excitation of a two-spheroid cluster results only in weak interaction between the nanospheroids (see the dispersion curves for the T-modes on Fig. 4(a)). Due to this weak interaction, absorption and scattering cross-sections for this polarization are approximately equal to doubled and quadrupled cross-sections of a single spheroid respectively. It is also interesting that plasmonic frequency of the  $L = 2$  mode is very close to plasmonic frequency of the  $T = 1$  mode. This fact can be easily understood from analysis of Fig. 4. Indeed, when width of the gap tends to zero, plasmonic frequency of  $L = 2$  modes also decreases to zero, while plasmonic frequency of the  $T = 1$  mode increases slightly. So, at some point these modes will intersect and have the same frequencies, and we observe this situation in Fig. 7.

It should be noticed that in Fig. 7 the maxima of absorption corresponding to plasmon oscillations of M-type again are not visible. It is related to the fact that M-modes interact with a homogeneous electric field weakly and can be effectively excited only by a source of radiation that is nonuniform in comparison with a size of the gap between nanoparticles<sup>57</sup> (see Fig. 3).

To control correctness and accuracy of our analytical calculations for a cluster of two oblate spheroids, we have also carried out finite element simulation of this system with Comsol Multiphysics® software. The results of this simulation are shown by the circles in Fig. 7. One can see that there is a fine agreement between the analytical and pure numerical calculations. This fact confirms correctness and accuracy of the both of approaches again.

### C. Enhancement of local fields

The most important characteristic of nanoparticles clusters is the factor of incident field enhancement in the gap between the nanoparticles. It is the characteristic that allows determining the excitation rate of molecules near the nanoparticles or intensity of surface-enhanced Raman scattering<sup>4</sup>. Moreover, achievement of high values of this factor is the main goal of optical nano-antennas development.

Distribution of squared electric field for the L=1 resonance in a cluster of two prolate spheroids is shown in Fig. 8, that shows that, indeed, the maximal field enhancement takes place in the gap between the nanoparticles on their surfaces. The field maxima are also present on the outer side of the cluster; however, field amplitude is essentially less there. According to general theorems for harmonic functions, the field maximum can be reached only on the region boundaries. In our case, the field maxima are reached in those points of the spheroids' surface where the distance between the spheroids is minimal.

Using Eqs. (10) and (17), one can find explicit expressions for the field enhancement factor  $G$ . For clusters of two identical prolate spheroids in the considered configuration (Fig. 1(a)), one can obtain the following expression for the field maximum in the case of an incident field polarized along the z-axis:

$$G = \frac{|\mathbf{E}|^2}{|E_{0z}|^2} = \left| 1 - \frac{1}{E_{0z}f} \sum_{n=1}^{\infty} C_{0n} \left( \frac{dQ_n(\xi_1)}{d\xi_1} + \frac{dQ_n(\xi_2)}{d\xi_2} \right) \right|^2, \quad (37)$$

where  $\xi_1 = c/f$  and  $\xi_2 = (l - c)/f$ , while  $C_{0n} = C_{0n}^{(1)} = -(-1)^n C_{0n}^{(2)}$ . In the most interesting case of a small gap and strongly prolate spheroids,  $\xi_1, \xi_2 \approx 1$ , and one may use the asymptotic form  $\left. \frac{dQ_n(\xi)}{d\xi} \right|_{\xi \approx 1} \approx -\frac{1}{2(\xi-1)}$ . As a result, the field enhancement factor takes the form:

$$G = \frac{|\mathbf{E}|^2}{|E_{0z}|^2} \approx \left| \frac{1}{2E_{0z}f} \left( \frac{1}{\xi_1 - 1} + \frac{1}{\xi_2 - 1} \right) \sum_{n=1}^{\infty} C_{0n} \right|^2. \quad (38)$$

In the case of clusters of two identical oblate spheroids (Fig. 1(b)) and incident field polarized along the x-axis, we obtain

$$G = \frac{|\mathbf{E}|^2}{|E_{0x}|^2} = \left| \frac{1}{E_{0x}f} \sum_{n=1}^{\infty} \sum_{m=0}^n C_{mn} \frac{dP_n^m(\eta)}{d\eta} \Big|_{\eta=0} \left( \frac{1}{\xi_1} Q_n^m(i\xi_1) - \frac{1}{\xi_2} Q_n^m(i\xi_2) \right) \right|^2 + \left| 1 - \frac{1}{E_{0x}f} \sum_{n=1}^{\infty} \sum_{m=0}^n C_{mn} P_n^m(0) \left( \sqrt{1 + \frac{1}{\xi_1^2}} \frac{dQ_n^m(i\xi_1)}{d\xi_1} + \sqrt{1 + \frac{1}{\xi_2^2}} \frac{dQ_n^m(i\xi_2)}{d\xi_2} \right) \right|^2, \quad (39)$$

where  $\xi_1 = \sqrt{a^2/f^2 - 1}$ ,  $\xi_2 = \sqrt{(l-a)^2/f^2 - 1}$ ;  $C_{mn} = -(-1)^m C_{mn}^{(1)} = C_{mn}^{(2)}$ .

In Fig. 9, the dependence of squared electric field enhancement (37) and (39) for clusters of two identical silver nanospheroids on the wavelength, is shown. Comparing peaks positions to the dispersion curves in Fig. 2 and Fig. 4, one can come to a conclusion that only ‘‘L’’ types of plasmon modes are excited in the clusters for the considered configurations of nanospheroids and incident electromagnetic wave polarizations (along the line joining the nanoparticles’ centers). In particular, excitation of the L = 1 and L = 2 modes is noticeable. At that, the position of squared field enhancement peaks agrees with the maxima of the absorption and scattering cross-sections shown in Fig. 6 and 7 by the solid lines z and x correspondingly. It should be mentioned that the value of squared field enhancement near a cluster of two nanospheroids can reach up to  $10^6$ . In the case of single nanoparticles, this value is almost two orders less than that of clusters (cf. the solid and dashed curves in Fig. 9). This fact determines a greater attractiveness of metal nanoparticles clusters in comparison to single nanoparticles for investigation of Surface Enhance Raman Scattering (SERS) and Surface-Enhanced Fluorescence (SEF). Let us note that the obtained great field enhancement factors can be slightly less in practice since for small particles and for small gaps between them, non-local and other effects not considered in this research become essential.

## IV. A CLUSTER OF TWO NANOSPHEROIDS IN THE FIELD OF A DIPOLE SOURCE

In the previous section, we have considered the case of a nano-antenna placed in the field of a plane wave. However, highly nonuniform optical fields occur very often in nano-environment. For example, such fields arise when a plasmonic nano-antenna is excited by an atom, or a molecule, or another nanolocalized source of light. So, in this section, we will consider an important case of a two-nanospheroid cluster in the field of electric dipole sources. Excitation of the cluster by magnetic dipole and electric quadrupole sources can be analyzed analogously.

### A. A cluster of two prolate nanospheroids

A case of two prolate nanospheroids in the field of a dipole source of radiation can be considered by perfect analogy with a case of the same cluster in a uniform field. One should again look for solution in the form (9), (10) and then apply the boundary conditions (25). The only difference is that now the external potential is the potential  $\varphi_0$  of the dipole that has the following form in the  $j$ -th local system of coordinates of a prolate spheroid<sup>55</sup> ( $j = 1, 2$ ):

$$\begin{aligned} \varphi_0^{(j)} &= (\mathbf{d}_0 \nabla'_j) \frac{1}{|\mathbf{r} - \mathbf{r}'|} \\ &= \sum_{n=0}^{\infty} \sum_{m=0}^n \begin{cases} P_n^m(\xi_j) P_n^m(\eta_j) \left[ (\mathbf{d}_0 \nabla'_j) \alpha_{mn}^{(j)} \cos(m\phi_j) + (\mathbf{d}_0 \nabla'_j) \beta_{mn}^{(j)} \sin(m\phi_j) \right], & \xi_j < \xi'_j, \\ Q_n^m(\xi_j) P_n^m(\eta_j) \left[ (\mathbf{d}_0 \nabla'_j) \gamma_{mn}^{(j)} \cos(m\phi_j) + (\mathbf{d}_0 \nabla'_j) \sigma_{mn}^{(j)} \sin(m\phi_j) \right], & \xi_j > \xi'_j. \end{cases} \end{aligned} \quad (40)$$

In Eq. (40),  $\mathbf{d}_0$  denotes the dipole momentum of a source placed at  $\mathbf{r}'$ ,  $\nabla'_j$  is a gradient over  $\mathbf{r}'$  in local coordinates, and

$$\begin{aligned} \left. \begin{matrix} \alpha_{mn}^{(j)} \\ \beta_{mn}^{(j)} \end{matrix} \right\} &= \frac{1}{f} (2 - \delta_{m0}) (-1)^m (2n + 1) \left[ \frac{(n - m)!}{(n + m)!} \right]^2 Q_n^m(\xi'_j) P_n^m(\eta'_j) \begin{cases} \cos(m\phi'_j) \\ \sin(m\phi'_j) \end{cases}, \\ \left. \begin{matrix} \gamma_{mn}^{(j)} \\ \sigma_{mn}^{(j)} \end{matrix} \right\} &= \frac{1}{f} (2 - \delta_{m0}) (-1)^m (2n + 1) \left[ \frac{(n - m)!}{(n + m)!} \right]^2 P_n^m(\xi'_j) P_n^m(\eta'_j) \begin{cases} \cos(m\phi'_j) \\ \sin(m\phi'_j) \end{cases}, \end{aligned} \quad (41)$$

are expansion coefficients of the unit charge potential in local coordinates of a prolate spheroid.

As a result of applying of the boundary conditions, one can obtain a system of equations for the unknown coefficients  $C_{mn}^{(j)}$ ,  $D_{mn}^{(j)}$  in Eq. (10). The new system can be easily derived from Eqs. (26) and (27) if one makes the following replacement for the coefficients  $a_{mn}^{(j)}$  and  $b_{mn}^{(j)}$ :

$$\begin{aligned} a_{mn}^{(1)} &= -(\mathbf{d}_0 \nabla'_1) \alpha_{mn}^{(1)}, & a_{mn}^{(2)} &= -(\mathbf{d}_0 \nabla'_2) \alpha_{mn}^{(2)}, \\ b_{mn}^{(1)} &= -(\mathbf{d}_0 \nabla'_1) \beta_{mn}^{(1)}, & b_{mn}^{(2)} &= -(\mathbf{d}_0 \nabla'_2) \beta_{mn}^{(2)}, \end{aligned} \quad (42)$$

where  $\alpha_{mn}^{(j)}$  and  $\beta_{mn}^{(j)}$  are defined by Eq. (41).

After Eqs. (26) and (27) have been solved with taking (42) into account, one can find the total induced dipole moment of the prolate nanospheroids

$$\begin{aligned} d_x &= \frac{2f^2}{3} (C_{11}^{(1)} + C_{11}^{(2)}), \\ d_y &= \frac{2f^2}{3} (D_{11}^{(1)} + D_{11}^{(2)}), \\ d_z &= \frac{f^2}{3} (C_{01}^{(1)} + C_{01}^{(2)}). \end{aligned} \quad (43)$$

Knowing the dipole momenta (43), it is easy to find radiative decay rate of a dipole placed near the prolate nanospheroid<sup>59</sup>:

$$\gamma = \frac{P^{rad}}{\hbar\omega} = \frac{\omega^3}{3\hbar v_c^3} |\mathbf{d}_0 + \mathbf{d}|^2. \quad (44)$$

where  $P^{rad}$  is radiation power at frequency  $\omega$  and  $\hbar\omega$  is emitted photon energy.

Radiative decay rate is a very important characteristics in such applications as surface enhanced Raman scattering, surface-enhanced fluorescence, nanolasers, and so on. To characterize the radiative decay rate, it is naturally to normalize it to radiative decay rate of a dipole in free space,  $\gamma_0 = \frac{P_0^{rad}}{\hbar\omega} = \frac{\omega^3}{3\hbar v_c^3} |\mathbf{d}_0|^2$ .

In Fig. 10, normalized radiative decay rate of a dipole source placed at the middle point of the gap is shown. As it is well seen in Fig. 10(a), if the distance between the prolate nanospheroids is small (Fig. 10(a), the curves  $\alpha$  and  $\delta$ ), the dipole source with a moment

oriented perpendicular to the cluster's axis of rotation, can excite both symmetrical T- and M-modes. This fact differs from the case of excitation of the same cluster with a plane wave, when M-modes with peaks located in the region of  $\lambda < 337$  nm (see Fig. 2(a)) are not excited. When the distance between the nanospheroids increases (see Fig. 10(a)), the peak corresponding to M-modes shifts to  $\lambda \approx 337$  nm ( $\omega \approx \omega_{pl}/\sqrt{2}$ ) and then disappears. After that point, only the peaks corresponding to plasmonic T-modes can be observed. Of course, this picture is in agreement with the behavior of the plasmonic M-modes shown in Fig. 2(a). We shall also notice that for large enough distances between the nanospheroids (see Fig. 10(a), the curve  $\gamma$ ) the self-consistent model<sup>3,21</sup>, in which nanoparticles are replaced by point dipoles with corresponding polarizabilities<sup>3,34</sup>, can be effectively used for calculation of radiative decay rate (the dashed curve).

When dipole moment of a source is oriented along the axis of symmetry (Fig. 10(b)), only antisymmetric L-modes can be excited due to symmetry reasons. From Fig. 10(b), one can also see that for small enough distances between the spheroids there are two plasmonic modes ( $L = 1, 2$ ) that interact with the dipole source. When the distance between the spheroids diminishes, further peaks of radiation power shift towards long wavelengths. At large distances between the nanospheroids, there is only one maximum corresponding to the  $L = 1$  plasmonic mode (see Fig. 10(b), the curve  $\gamma$ ). In this case, the radiative decay rate of a dipole placed near a cluster of two prolate nanospheroids can be also calculated with making use of the self-consistent analytical model in which the spheroids are approximated by point dipoles (see the dashed curve in Fig. 10(b)).

## B. A cluster of two oblate nanospheroids

A case of two oblate nanospheroids in the field of a dipole source of radiation can be considered by perfect analogy with a case of the same cluster in a uniform field. One should again look for solution in the forms (16) and (17) and then apply the boundary conditions (25). The only difference is that now the external potential is the potential  $\varphi_0$  of the dipole that has the following form in the  $j$ -th local system of coordinates of an oblate spheroid<sup>55</sup> ( $j = 1, 2$ ):

$$\begin{aligned}
\varphi_0^{(j)} &= (\mathbf{d}_0 \nabla'_j) \frac{1}{|\mathbf{r} - \mathbf{r}'|} \\
&= \sum_{n=0}^{\infty} \sum_{m=0}^n \begin{cases} P_n^m(i\xi_j) P_n^m(\eta_j) \left[ (\mathbf{d}_0 \nabla'_j) \alpha_{mn}^{(j)} \cos(m\phi_j) + (\mathbf{d}_0 \nabla'_j) \beta_{mn}^{(j)} \sin(m\phi_j) \right], & \xi_j < \xi'_j, \\ Q_n^m(i\xi_j) P_n^m(\eta_j) \left[ (\mathbf{d}_0 \nabla'_j) \gamma_{mn}^{(j)} \cos(m\phi_j) + (\mathbf{d}_0 \nabla'_j) \sigma_{mn}^{(j)} \sin(m\phi_j) \right], & \xi_j > \xi'_j. \end{cases}
\end{aligned} \tag{45}$$

In Eq. (45),  $\mathbf{d}_0$  denotes the dipole momentum of a source placed at  $\mathbf{r}'$ ,  $\nabla'_j$  is gradient over  $\mathbf{r}'$  in local coordinates, and

$$\begin{aligned}
\left. \begin{array}{l} \alpha_{mn}^{(j)} \\ \beta_{mn}^{(j)} \end{array} \right\} &= \frac{i}{f} (2 - \delta_{m0}) (-1)^m (2n + 1) \left[ \frac{(n - m)!}{(n + m)!} \right]^2 Q_n^m(i\xi'_j) P_n^m(\eta'_j) \begin{cases} \cos(m\phi'_j) \\ \sin(m\phi'_j) \end{cases}, \\
\left. \begin{array}{l} \gamma_{mn}^{(j)} \\ \sigma_{mn}^{(j)} \end{array} \right\} &= \frac{i}{f} (2 - \delta_{m0}) (-1)^m (2n + 1) \left[ \frac{(n - m)!}{(n + m)!} \right]^2 P_n^m(i\xi'_j) P_n^m(\eta'_j) \begin{cases} \cos(m\phi'_j) \\ \sin(m\phi'_j) \end{cases}, \tag{46}
\end{aligned}$$

are expansion coefficients of the unit charge potential in local coordinates of an oblate spheroid.

As a result of applying of the boundary conditions, one can obtain the system of equations for the unknown coefficients  $C_{mn}^{(j)}$ ,  $D_{mn}^{(j)}$  in Eq. (17). The system of equations for these coefficients can be easily derived from Eqs. (33) and (34) if one makes the following replacement for the coefficients  $a_{mn}^{(j)}$  and  $b_{mn}^{(j)}$

$$\begin{aligned}
a_{mn}^{(1)} &= -i (\mathbf{d}_0 \nabla'_1) \alpha_{mn}^{(1)}, & a_{mn}^{(2)} &= -i (\mathbf{d}_0 \nabla'_{21}) \alpha_{mn}^{(2)}, \\
b_{mn}^{(1)} &= -i (\mathbf{d}_0 \nabla'_1) \beta_{mn}^{(1)}, & b_{mn}^{(2)} &= -i (\mathbf{d}_0 \nabla'_2) \beta_{mn}^{(2)},
\end{aligned} \tag{47}$$

where  $\alpha_{mn}^{(j)}$  and  $\beta_{mn}^{(j)}$  are defined in Eq. (46).

The total induced dipole moment of a cluster of two oblate nanospheroids can be found by using the following expressions (cf. Eq. (43)):

$$\begin{aligned}
d_x &= -\frac{2f^2}{3} (C_{11}^{(1)} + C_{11}^{(2)}), \\
d_y &= -\frac{2f^2}{3} (D_{11}^{(1)} + D_{11}^{(2)}), \\
d_z &= -\frac{f^2}{3} (C_{01}^{(1)} + C_{01}^{(2)}).
\end{aligned} \tag{48}$$

In Fig. 11, normalized radiative decay rate of a dipole placed at the middle point between the oblate nanospheroids is shown. As one can see in Fig. 11(a), if dipole moment of a source is oriented along the line connecting the oblate nanospheroids' centers, only plasmonic L-modes are excited as it took place for the case of a cluster of two prolate nanospheroids (cf. Fig. 10(b)). When the distance between the nanospheroids is large enough (the  $\gamma$  curve), the properties of radiative decay of a dipole source located near the cluster can be more and more precisely approximated by means of the self-consistent model where spheroids are modeled by point dipoles (see Fig. 11(a), the dashed curve).

From Fig. 11(b) and (c) that correspond to the case of dipole moment of a source oriented along the y and z axes, one can conclude that only symmetric T-modes are presented here. Nevertheless, at small enough distances between the nanospheroids one can expect that M-modes are also excited but can not be seen due to large losses (large imaginary part of dielectric permittivity) in silver spheroids. If the imaginary part of permittivity of spheroidal nanoparticles' material is small enough, for example, in a case of silicized carbon (SiC)<sup>60</sup>, all fine features of the spectra and M-modes in particular will be well visible as it was demonstrated in<sup>20,21</sup> by the example of a cluster of two spheres.

## V. CONCLUSION

Thus, in the present work optical properties of clusters made of two metal nanospheroids are considered theoretically, and analytical results are obtained. This investigation has become possible due to proving of the addition translation theorem for spheroidal functions in quasistatic regime. Plasmonic eigenoscillations were analyzed in details, and it was found that in a cluster of two prolate or oblate nanospheroids there can be three types of plasmon modes. Two of them (low frequency,  $0 < \omega < \omega_{pl}/\sqrt{2}$ , L- and T-modes) can be effectively excited by a plane electromagnetic wave, while the third type (high frequency,  $\omega_{pl}/\sqrt{2} < \omega < \omega_{pl}$ , M-modes) can be excited only by a strongly nonuniform field of a nanolocalized source of light (a molecule, a quantum dot) located in the gap between two adjacent nanoparticles.

We have also investigated excitation of a nano-antenna made from two silver nanospheroids by fields of a plane wave and an electric dipole. The results of these investigations allow us to find absorption and scattering cross-sections of the nano-antenna as a function of wavelength for various polarization of an incident plane electromagnetic wave and to at-

tribute all observable peaks to excitation of corresponding plasmonic modes. We have also analyzed radiative decay rate (or local density of state) of a dipole placed in the gap between the nanospheroids and have attributed all observable peaks to excitation of corresponding plasmonic modes.

The obtained analytical results can be used in many applications based on plasmonic nano-antennas and on enhancement of local field (SERS, SEF, nanolasers, nano-optical circuits, and so on). Besides, our results are very important for controlling accuracy of different computational software that has no a priori test of accuracy.

## ACKNOWLEDGMENTS

The authors thank Russian Foundation of Basic Researches (grant 09-02-13560) for financial support. The authors also express their gratitude to Ulrike Woggon for her helpful comments.

## Appendix: Translational addition theorem for spheroidal wave functions in a quasistatic limit

A solution of the Helmholtz equation in spheroidal coordinates can be expanded as a series in spheroidal wave functions<sup>52</sup>. In spite of the fact that these functions are thoroughly studied<sup>51–54,56</sup>, the problem of electromagnetic waves scattering on a spheroid still remains one of the most complex ones, first of all, due to mathematical aspects related to usage of spheroidal wave functions. On the other hand, it is well-known that in a case of spheroids which size is substantially less than the wavelength (quasistatic limit), a solution of the Laplace equation in spheroidal coordinates can be presented as a series in associated Legendre functions<sup>55</sup>. The Legendre functions are widespread and included as standard special functions in majority of mathematical software programs, such as *Maple*, *Mathematica*, *MatLAB*, etc. That is why it is important to obtain the translational addition theorem for spheroidal wave functions in the case when sizes of spheroids are far less than the wavelength in which these functions would be “replaced” by corresponding Legendre functions.

In<sup>45</sup>, a rotational-translational addition theorem was obtained for spheroidal wave functions in a case of an arbitrary size of spheroids in comparison to the wavelength. This

theorem was derived in the following manner: first, spheroidal wave functions were expanded over spherical wave functions, then the spherical wave functions were expanded over spheroidal ones. Substituting one expansion into the other and using the addition theorem for spherical wave functions<sup>51,61</sup>, the required theorem for spheroidal functions was derived as a result. Here, we will do the same in a particular case when spheroids' sizes are far less than the wavelength.

In a case of a prolate spheroid, we have the following expansions<sup>45</sup>

$$\begin{aligned} & R_{mn}^{(3)}(kf, \xi) S_{mn}^{(1)}(kf, \eta) e^{im\phi} \\ &= \sum_{q=|m|, |m|+1}^{\infty} i^{q-n} d_{q-|m|}^{mn}(kf) h_q^{(1)}(kr) P_q^m(\cos \theta) e^{im\phi}, \end{aligned} \quad (\text{A.1})$$

where  $1 \leq \xi < \infty$ ,  $-1 \leq \eta \leq 1$  and  $0 \leq \phi \leq 2\pi$  are coordinates of the prolate spheroid<sup>52</sup>;  $0 \leq r < \infty$ ,  $0 \leq \theta \leq \pi$  and  $0 \leq \phi \leq 2\pi$  are spherical coordinates;  $R_{mn}^{(3)}(kf, \xi)$  and  $S_{mn}^{(1)}(kf, \eta)$  are radial and angular spheroidal functions of the third and first kinds according to<sup>52</sup>;  $h_q^{(1)}(kr)$ , and  $P_q^m(\cos \theta)$  are the spherical Hankel function of the first kind<sup>56</sup> and the associated Legendre function<sup>56</sup>;  $d_{q-|m|}^{mn}(kf)$  are the expansion coefficients<sup>52</sup>;  $k$  is wavenumber,  $f$  is a half of the spheroid's focal distance; the stroke of the sum character implies summation over only even or only odd values of  $q$ . Another important relation from<sup>45</sup> has the form:

$$\begin{aligned} & j_n(kr) P_n^m(\cos \theta) e^{im\phi} = \frac{2}{2n+1} \frac{(n+m)!}{(n-m)!} \\ & \times \sum_{q=|m|, |m|+1}^{\infty} i^{q-n} \frac{1}{N_{mq}(kf)} d_{n-|m|}^{mq}(kf) R_{mq}^{(1)}(kf, \xi) S_{mq}^{(1)}(kf, \eta) e^{im\phi}, \end{aligned} \quad (\text{A.2})$$

where  $j_n(kr)$  is the spherical Bessel function<sup>56</sup>;  $R_{mq}^{(1)}(kf, \xi)$  is a radial spheroidal function of the first kind<sup>52</sup>, and  $N_{mq}(kf)$  is normalization factor of angular spheroidal functions of the first kind<sup>52</sup>. In the case of a spheroid which size is far less than the wavelength, that is, in the case  $k \rightarrow 0$ , one can use the following asymptotic expressions<sup>51</sup>:

$$\begin{aligned} d_{n-m-2q}^{mn} &\approx \frac{(n+m)!(2n-4q+1)!!(2n-2q-1)!!}{(n+m-2q)!(2n+1)!!(2q)!!(2n-1)!!} (kf)^{2q}, \quad 0 \leq q \leq \frac{n-m}{2}, \\ d_{n-m+2q}^{mn} &\approx \frac{(-1)^q (n-m+2q)!(2n-1)!!(2n+1)!!}{(n-m)!(2n+4q-1)!!(2q)!!(2n+2q+1)!!} (kf)^{2q}, \quad q \geq 1, \end{aligned} \quad (\text{A.3})$$

and  $N_{mn} \approx \frac{2}{2n+1} \frac{(n+m)!}{(n-m)!}$ . Radial and angular spheroidal functions  $R_{mn}^{(1)}(kf, \xi)$ ,  $R_{mn}^{(3)}(kf, \xi)$  and  $S_{mn}^{(1)}(kf, \eta)$  can be also presented in the asymptotic form<sup>51,53</sup>

$$\begin{aligned} R_{mn}^{(1)}(kf, \xi) &\approx \frac{(n-m)!}{(2n-1)!!(2n+1)!!} (kf)^n P_n^m(\xi), \\ R_{mn}^{(3)}(kf, \xi) &\approx -i \frac{(-1)^m (2n-1)!!(2n+1)!!}{(n+m)!} (kf)^{-n-1} Q_n^m(\xi), \\ S_{mn}^{(1)}(kf, \eta) &\approx P_n^m(\eta), \end{aligned} \quad (\text{A.4})$$

where  $P_n^m(\eta)$  is the associated Legendre function<sup>56</sup> defined on the segment  $-1 \leq \eta \leq 1$ ;  $P_n^m(\xi)$ ,  $Q_n^m(\xi)$  are associated Legendre functions of the first and second kinds<sup>56</sup>, correspondingly, defined in a complex plane with branch cut from  $-\infty$  to  $+1$ . Finally, asymptotic forms for spherical Bessel and Henkel functions have the form<sup>56</sup>:

$$j_n(kr) \approx \frac{2^n n!}{(2n+1)!} (kr)^n, \quad h_n^{(1)}(kr) \approx -i \frac{(2n)!}{2^n n!} (kr)^{-n-1}. \quad (\text{A.5})$$

Making use of Eqs. (A.3)-(A.5), one can obtain the following relations from Eqs. (A.1) and (A.2):

$$\begin{aligned} Q_n^m(\xi) P_n^m(\eta) &= \sum_{q=0}^{\infty} \frac{(-1)^m (n-m+2q)! (n+m)!}{(n-m)! (2n+2q+1)!! (2q)!!} \left(\frac{f}{r}\right)^{n+2q+1} P_{n+2q}^m(\cos \theta), \\ \left(\frac{r}{f}\right)^n P_n^m(\cos \theta) &= \frac{(n-m)!}{(2n-1)!!} P_n^m(\xi) P_n^m(\eta) \\ &+ \sum_{q=0,1}^{n-m-2} \frac{(n+m)! (2m+2q+1) q!}{(n-m-q)!! (n+m+q+1)!! (2m+q)!} P_{m+q}^m(\xi) P_{m+q}^m(\eta). \end{aligned} \quad (\text{A.6})$$

To obtain the required addition theorem for wave functions of prolate spheroids which size is far less than the wavelength from Eq. (A.6), it is necessary to apply the corresponding theorem for spherical wave functions<sup>19</sup>:

$$\begin{aligned} \left(\frac{l}{r_j}\right)^{n+1} P_n^m(\cos \theta_j) e^{im\phi_j} &= \sum_{q=0}^{\infty} \sum_{p=-q}^q R_{pqmn}(\theta_{js}, \phi_{js}) \left(\frac{r_s}{l}\right)^q P_q^p(\cos \theta_s) e^{ip\phi_s}, \\ R_{pqmn}(\theta_{js}, \phi_{js}) &= \frac{(-1)^{q+m} (q+n-p+m)!}{(q+p)! (n-m)!} P_{q+n}^{p-m}(\cos \theta_{js}) e^{i(m-p)\phi_{js}}. \end{aligned} \quad (\text{A.7})$$

In the expression (A.7), the indices  $j, s = 1, 2$  ( $j \neq s$ ) denote the first “1” and the second “2” local systems of spherical coordinates, that are based on local Cartesian coordinates with parallel axes and attached to the spheres’ centers;  $(r_{js}, \theta_{js}, \phi_{js})$  are spherical coordinates of the origin of the  $s$ -th coordinate system in the  $j$ -th local system of coordinates;  $l = r_{js} = r_{sj}$  is the distance between the origins of local coordinates systems (see Fig. 12). Substituting Eq. (A.7) into Eq. (A.6), we obtain after series of transformations the required translational addition theorem for wave functions of prolate spheroids in the quasistatic limit:

$$\begin{aligned}
Q_n^m(\xi_j) P_n^m(\eta_j) e^{im\phi_j} &= \sum_{q=0}^{\infty} \sum_{p=-q}^q O_{pqmn}(f_j, f_s, l, \theta_{js}, \phi_{js}) P_q^p(\xi_s) P_q^p(\eta_s) e^{ip\phi_s}, \\
O_{pqmn}(f_j, f_s, l, \theta_{js}, \phi_{js}) &= \frac{(-1)^q (2q+1)(q-p)!(n+m)!}{(q+p)!(n-m)!} \\
&\times \sum_{r=0}^{\infty} \sum_{k=0}^{\infty} \frac{(q+n+2r+2k-p+m)!}{(2q+2r+1)!!(2n+2k+1)!!(2r)!!(2k)!!} \\
&\times \left(\frac{f_s}{l}\right)^{2r+q} \left(\frac{f_j}{l}\right)^{2k+n+1} P_{q+n+2r+2k}^{p-m}(\cos\theta_{js}) e^{i(m-p)\phi_{js}}. \tag{A.8}
\end{aligned}$$

In Eq. (A.8), the indices  $j, s = 1, 2$  ( $j \neq s$ ) denote the first and second local prolate spheroid coordinate systems with the parallel Cartesian axes introduced above; the spherical angles  $\theta_{js}$  and  $\phi_{js}$  are the same as in Eq. (A.7);  $l$  is the distance between the origins of local coordinate systems (see Fig. 12 for details). Let us add that an obligatory condition for usage of the theorem (A.8) is parallelism of Cartesian axes in the local coordinate systems. In the case when the second local coordinate system is turned around the first one, the theorem (A.7) is to be changed<sup>19</sup>, resulting in corresponding modification of the theorem (A.8). Let us also note that mathematical applicability condition for (A.8) is convergence of the series in this expression. In particular, one may state that Eq. (A.8) is applicable in the case of non-overlapping spheroids<sup>51</sup>.

The translational addition theorem for functions of oblate spheroids which size is much less than the wavelength, can be obtained from Eq. (A.8) if the formal substitution is used<sup>52</sup>:  $\xi \rightarrow i\xi$  and  $f \rightarrow -if$ . In expressions derived in this manner,  $\xi$  is a coordinate in the system of the oblate spheroid ( $0 \leq \xi < \infty$ );  $f$  is a half of the focal distance of the oblate spheroid. Let us note that (A.8) is a very general theorem, and many other theorems relating prolate, oblate, and spherical functions can be derived from it.

The obtained theorem (A.8) is not very convenient for numerical calculations since it contains summation both over positive and negative  $p$ . To simplify it, let us use properties of the associated Legendre functions<sup>51,62</sup>, basing on which we shall find that

$$\begin{aligned} & O_{-p,q,-m,n}(f_j, f_s, l, \theta_{js}, \phi_{js}) \\ &= (-1)^{p-m} \left[ \frac{(q+p)!(n-m)!}{(q-p)!(n+m)!} \right]^2 O_{pqmn}(f_j, f_s, l, \theta_{js}, \phi_{js}) e^{i2(p-m)\phi_{js}}. \end{aligned} \quad (\text{A.9})$$

Combining Eqs. (A.8) and (A.9), one can derive the following relation ( $m, p = 0, 1, 2, \dots$ ):

$$\begin{aligned} Q_n^m(\xi_j) P_n^m(\eta_j) & \begin{cases} \cos(m\phi_j) \\ \sin(m\phi_j) \end{cases} = \sum_{q=0}^{\infty} \sum_{p=0}^q P_q^p(\xi_s) P_q^p(\eta_s) \\ & \times \begin{cases} L_{pqmn}(f_j, f_s, l, \theta_{js}) \cos(p\phi_s - (p-m)\phi_{js}) \\ L_{pqmn}(f_j, f_s, l, \theta_{js}) \sin(p\phi_s - (p-m)\phi_{js}) \\ + T_{pqmn}(f_j, f_s, l, \theta_{js}) \cos(-p\phi_s + (p+m)\phi_{js}) \\ + T_{pqmn}(f_j, f_s, l, \theta_{js}) \sin(-p\phi_s + (p+m)\phi_{js}) \end{cases}, \end{aligned} \quad (\text{A.10})$$

where

$$\begin{aligned} L_{pqmn}(f_j, f_s, l, \theta_{js}) &= \frac{(-1)^q (2 - \delta_{0p}) (2q+1) (q-p)! (n+m)!}{2 (q+p)! (n-m)!} \\ & \times \sum_{r=0}^{\infty} \sum_{k=0}^{\infty} \frac{(q+n+2r+2k-p+m)!}{(2q+2r+1)!! (2n+2k+1)!! (2r)!! (2k)!!} \\ & \times \left( \frac{f_s}{l} \right)^{2r+q} \left( \frac{f_j}{l} \right)^{2k+n+1} P_{q+n+2r+2k}^{p-m}(\cos \theta_{js}), \\ T_{pqmn}(f_j, f_s, l, \theta_{js}) &= \frac{(-1)^{q+m} (2 - \delta_{0p}) (2q+1) (q-p)! (n+m)!}{2 (q+p)! (n-m)!} \\ & \times \sum_{r=0}^{\infty} \sum_{k=0}^{\infty} \frac{(q+n+2r+2k-p-m)!}{(2q+2r+1)!! (2n+2k+1)!! (2r)!! (2k)!!} \\ & \times \left( \frac{f_s}{l} \right)^{2r+q} \left( \frac{f_j}{l} \right)^{2k+n+1} P_{q+n+2r+2k}^{p+m}(\cos \theta_{js}), \end{aligned} \quad (\text{A.11})$$

and  $\delta_{0p}$  is Kronecker delta symbol.

In the case of coaxial prolate spheroids with a common axis  $z$ , one should take  $\phi_j = \phi_s$  and  $\theta_{js} = 0$  or  $\theta_{js} = \pi$  in Eq. (A.10). This results in the following relation ( $m = 0, 1, 2, \dots$ ):

$$\begin{aligned}
Q_n^m(\xi_j) P_n^m(\eta_j) &= \sum_{q=m}^{\infty} S_{mqmn}(f_j, f_s, l, \theta_{js}) P_q^m(\xi_s) P_q^m(\eta_s), \\
S_{mqmn}(f_j, f_s, l, \theta_{js}) &= \frac{(-1)^q (2q+1)(q-m)!(n+m)!}{(q+m)!(n-m)!} P_{q+n}(\cos \theta_{js}) \\
&\times \sum_{r=0}^{\infty} \sum_{k=0}^{\infty} \frac{(q+n+2r+2k)!}{(2q+2r+1)!!(2n+2k+1)!!(2r)!!(2k)!!} \left(\frac{f_s}{l}\right)^{2r+q} \left(\frac{f_j}{l}\right)^{2k+n+1}.
\end{aligned} \tag{A.12}$$

In the case when local coordinate systems of the spheroids have a common axis  $x$ , one should take  $\theta_{js} = \pi/2$  and  $\phi_{js} = 0$  or  $\phi_{js} = \pi$  in Eq. (A.10). As a result, we have in this case

$$\begin{aligned}
Q_n^m(\xi_j) P_n^m(\eta_j) &\begin{cases} \cos(m\phi_j) \\ \sin(m\phi_j) \end{cases} \\
&= \sum_{q=0}^{\infty} \sum_{p=0}^q P_q^p(\xi_s) P_q^p(\eta_s) \begin{cases} M_{pqmn}(f_j, f_s, l, \phi_{js}) \cos(p\phi_s) \\ N_{pqmn}(f_j, f_s, l, \phi_{js}) \sin(p\phi_s) \end{cases},
\end{aligned} \tag{A.13}$$

where

$$\begin{aligned}
&M_{pqmn}(f_j, f_s, l, \phi_{js}) \\
&= (L_{pqmn}(f_j, f_s, l, \pi/2) + T_{pqmn}(f_j, f_s, l, \pi/2)) \cos((p-m)\phi_{js}), \\
&N_{pqmn}(f_j, f_s, l, \phi_{js}) \\
&= (L_{pqmn}(f_j, f_s, l, \pi/2) - T_{pqmn}(f_j, f_s, l, \pi/2)) \cos((p-m)\phi_{js}).
\end{aligned} \tag{A.14}$$

To simplify Eq. (A.14), it is convenient to use the relation<sup>56</sup>:

$$P_n^m(0) = \frac{2^m}{\sqrt{\pi}} \cos\left((n+m)\frac{\pi}{2}\right) \frac{\Gamma((n+m+1)/2)}{\Gamma((n-m+2)/2)}, \tag{A.15}$$

where  $\Gamma(x)$  is Euler's gamma function<sup>56</sup>.

---

\* guzatov@gmail.com

<sup>†</sup> vklim@sci.lebedev.ru

- <sup>1</sup> H. Raether, *Surface Plasmons on Rough and Smooth Surfaces and on Gratings* (Springer-Verlag, Berlin, 1998).
- <sup>2</sup> S.A. Maier, *Plasmonics: Fundamentals and Applications* (Springer, New York, 2007).
- <sup>3</sup> V.V. Klimov, *Nanoplasmonics* [in Russian] (Fizmatlit, Moscow, 2009).
- <sup>4</sup> *Surface-Enhanced Raman Scattering*, K. Kneipp, M. Moskovits, H. Kneipp (eds.) (Springer-Verlag, Berlin, 2006).
- <sup>5</sup> Y. Liu, J. Bishop, L. Williams, S. Blair, and J. Herron, *Nanotechnology* **15**, 1368 (2004).
- <sup>6</sup> A.J. Haes, S.L. Zou, G.C. Schatz, and R.P. van Duyne, *J. Phys. Chem. B* **108**, 6961 (2004).
- <sup>7</sup> A.J. Haes, S.L. Zou, G.C. Schatz, and R.P. van Duyne, *J. Phys. Chem. B* **108**, 109 (2004).
- <sup>8</sup> S. Chah, M.R. Hammond, R.N. Zare, *Chemistry and Biology* **12**, 323 (2005).
- <sup>9</sup> C. Sonnichsen, B.M. Reinhard, J. Liphardt, and A.P. Alivisatos, *Nat. Biotechnol.* **23**, 741 (2005).
- <sup>10</sup> J.N. Farahani, D.W. Pohl, H.-J. Eisler, and B. Hecht, *Phys. Rev. Lett.* **95**, 017402 (2005).
- <sup>11</sup> P. Muhlschlegel, H.-J. Eisler, O.J.F. Martin, B. Hecht, and D.W. Pohl, *Science* **308**, 1607 (2005).
- <sup>12</sup> L. Novotny, *Phys. Rev. Lett.* **98**, 266802 (2007).
- <sup>13</sup> T.H. Taminiau, F.D. Stefani, and N.F. van Hulst, *Opt. Exp.* **16**, 10858 (2008).
- <sup>14</sup> H. Fischer and O.J.F. Martin, *Opt. Exp.* **16**, 9144 (2008).
- <sup>15</sup> J.R. Lakowicz, J. Malicka, I. Gryczynski, Z. Gryczynski and C.D. Geddes, *J. Phys. D: Appl. Phys.* **36**, R240 (2003).
- <sup>16</sup> R. Ruppin, *J. Chem. Phys.* **76**, 1681 (1982).
- <sup>17</sup> R. Ruppin, *Phys. Rev. B* **26**, 3440 (1982).
- <sup>18</sup> F. Claro, *Phys. Rev. B* **25**, 7875 (1982).
- <sup>19</sup> J.M. Gerardy and M. Ausloos, *Phys. Rev. B* **22**, 4950 (1980).
- <sup>20</sup> V.V. Klimov and D.V. Guzatov, *Phys. Rev. B* **75**, 024303 (2007).
- <sup>21</sup> V.V. Klimov, D.V. Guzatov, *Quantum Electron.* **37**, 209 (2007).
- <sup>22</sup> P. Chu and D.L. Mills, *Phys. Rev. B* **77**, 045316 (2008).
- <sup>23</sup> K. Li, M.I. Stockman, and D.J. Bergman, *Phys. Rev. Lett.* **91**, 227402 (2003).
- <sup>24</sup> D.A. Genov, A.K. Sarychev, V.M. Shalaev, and A. Wei, *Nano Lett.* **4**, 153 (2004).
- <sup>25</sup> P. Nordlander and C. Oubre, E. Prodan, K. Li and M.I. Stockman, *Nano Lett.* **4**, 899 (2004).

- <sup>26</sup> I. Romero, J. Aizpurua, G.W. Bryant, F.J. Garcia de Abajo, *Opt. Exp.* **14**, 9988 (2006).
- <sup>27</sup> M. Danckwerts and L. Novotny, *Phys. Rev. Lett.* **98**, 026104 (2007).
- <sup>28</sup> M. Quinten, A. Leitner, J.R. Krenn, and F.R. Aussenegg, *Opt. Lett.* **23**, 1331 (1998).
- <sup>29</sup> S.A. Maier, P.G. Kik, and H.A. Atwater, *Appl. Phys. Lett.* **81**, 1714 (2002).
- <sup>30</sup> D.-S. Wang and M. Kerker, *Phys. Rev. B* **24**, 1777 (1981).
- <sup>31</sup> V.V. Klimov, M. Ducloy, and V.S. Letokhov, *Eur. Phys. J. D* **20**, 133 (2002).
- <sup>32</sup> A. Trugler and U. Hohenester, *Phys. Rev. B* **77**, 115403 (2008).
- <sup>33</sup> A.F. Stevenson, *J. Appl. Phys.* **24**, 1143 (1953).
- <sup>34</sup> D.V. Guzatov, V.V. Klimov, *Chem. Phys. Lett.* **412**, 341 (2005).
- <sup>35</sup> J. Grand, P.-M. Adam, A.-S. Grimault, A. Vial, M. Lamy de la Chapelle, J.-L. Bijeon, S. Kostcheev and P. Royer, *Plasmonics* **1**, 135 (2006).
- <sup>36</sup> D.V. Guzatov, V.V. Klimov, and M.Yu. Pikhota, *Laser Phys.* **10**, 85 (2010).
- <sup>37</sup> *Surface Plasmon Nanophotonics*, M.L. Brongersma, P.G. Kik (eds.) (Springer, Dordrecht, 2007).
- <sup>38</sup> S.A. Maier, M.L. Brongersma, P.G. Kik, S. Meltzer, A.A.G. Requicha, and H.A. Atwater, *Adv. Mater.* **13**, 1501 (2001).
- <sup>39</sup> O.L. Muskens, V. Giannini, J.A. Sanchez-Gil, J. Gomez Rivas, *Opt. Exp.* **15**, 17736 (2007).
- <sup>40</sup> W. Rechberger, A. Hohenau, A. Leitner, J.R. Krenn, B. Lamprecht, F.R. Aussenegg, *Optics Comm.* **220**, 137 (2003).
- <sup>41</sup> E. Cubukcu, F. Degirmenci, C. Kocabas, M.A. Zimmler, J.A. Rogers, and F. Capasso, *Proc. Nat. Acad. Sc.* **106**, 2495 (2009).
- <sup>42</sup> V. Poponin, A. Ignatov, *J. Kor. Phys. Soc.* **47**, 222 (2005).
- <sup>43</sup> L. Rogobete, F. Kaminski, M. Agio, and V. Sandoghdar, *Opt. Lett.* **32**, 1623 (2007).
- <sup>44</sup> A. Ghoshal and P.G. Kik, *J. Appl. Phys.* **103**, 113111 (2008).
- <sup>45</sup> R.H. MacPhie, J. Dalmas, and R. Deleuil, *Quart. Appl. Math.* **XLIV**, 737 (1987).
- <sup>46</sup> J. Dalmas, R. Deleuil and R.H. MacPhie, *Quart. Appl. Math.* **XLVII**, 351 (1989).
- <sup>47</sup> M.F.R. Cooray and I.R. Ciric, *IEEE Trans. Antennas Propag.* **37**, 608 (1989).
- <sup>48</sup> M.F.R. Cooray and I.R. Ciric, *Computer Phys. Comm.* **68**, 279 (1991).
- <sup>49</sup> P.B. Johnson, R.W. Christy, *Phys. Rev. B* **6**, 4370 (1972).
- <sup>50</sup> N.N. Voitovich, B.Z. Katsenelenbaum, A.N. Sivov, *Generalized Method of Eigen-Oscillations in the Theory of Diffraction* [in Russian] (Nauka, Moscow, 1977).
- <sup>51</sup> E.A. Ivanov, *Diffraction of Electromagnetic Waves on Two Bodies* [in Russian] (Nauka i

- Tekhnika, Minsk, 1969).
- <sup>52</sup> C. Flammer, *Spheroidal Wave Functions* (Stanford University Press, Stanford, 1957).
- <sup>53</sup> I.V. Komarov, L.I. Ponomaryev, S.Yu. Slavyanov, *Spheroidal and Coulomb's Spheroidal Functions* [in Russian] (Nauka, Moscow, 1976).
- <sup>54</sup> L.-W. Li, X.-K. Kang, M.-S. Leong, *Spheroidal Wave Functions in Electromagnetic Theory* (John Wiley and Sons, New York, 2002).
- <sup>55</sup> W.R. Smythe, *Static and Dynamic Electricity* (McGraw-Hill, New York, 1950).
- <sup>56</sup> M. Abramowitz and I.A. Stegun, *Handbook of Mathematical Functions* (Dover, New York, 1965).
- <sup>57</sup> V.V. Klimov, D.V. Guzatov, *Appl. Phys. A* **89**, 305 (2007).
- <sup>58</sup> L.D. Landau and E.M. Lifshits, *Electrodynamics of Continuous Media* [in Russian] (Nauka, Moscow, 1982).
- <sup>59</sup> V.V. Klimov, M. Ducloy, *Phys. Rev. A* **69**, 013812 (2004).
- <sup>60</sup> F. Engelbrecht and R. Helbig, *Phys. Rev. B* **48**, 698 (1993).
- <sup>61</sup> B. Friedman and J. Russek, *Quart. Appl. Math.* **XII**, 13 (1954).
- <sup>62</sup> I.S. Gradshteyn and I.M. Ryzhik, *Tables of Integrals, Sums, Series and Products* [in Russian] (Fizmatgiz, Moscow, 1963).

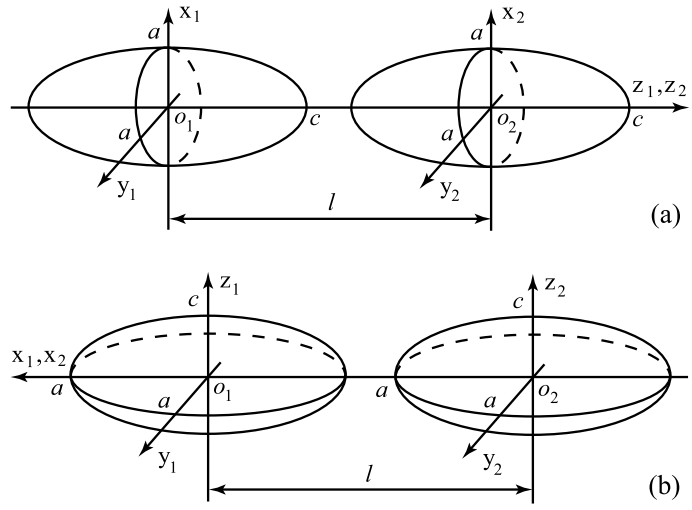


FIG. 1. The geometry of a two-nanospheroid cluster. (a) The case of prolate nanospheroids, (b) the case of oblate nanospheroids.

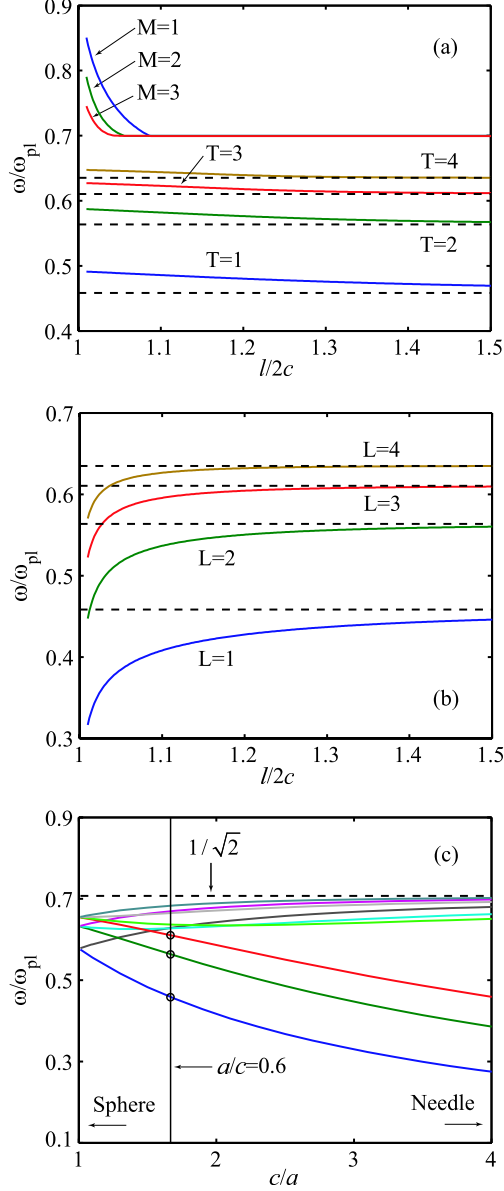


FIG. 2. (Color online) Normalized frequencies of the first three plasmonic oscillations in a cluster of two identical prolate spheroidal nanoparticles as a function of the distance between the nanospheroids' centers. The axis-symmetrical case ( $m = 0$ ) is considered, and the aspect ratio of a single spheroid is  $a/c = 0.6$  ( $\xi_0 = 1/\sqrt{1 - (a/c)^2}$ ). (a) Symmetrical modes (eigenvalues of Eq. (14)), (b) antisymmetrical modes (eigenvalues of Eq. (15)). Dashed lines show plasmon frequencies of a single prolate nanospheroid  $\frac{\omega}{\omega_{pl}} = \left\{ \frac{dP_n^m(\xi_0)}{d\xi_0} Q_n^m(\xi_0) / \left( \frac{dP_n^m(\xi_0)}{d\xi_0} Q_n^m(\xi_0) - P_n^m(\xi_0) \frac{dQ_n^m(\xi_0)}{d\xi_0} \right) \right\}^{1/2}$ . The figure (c) shows plasmon frequencies of the single prolate nanospheroid as a function of the inverse aspect ratio  $c/a$ . The vertical line corresponds to  $a/c = 0.6$  and allows to select asymptotic values for the figures (a) and (b).

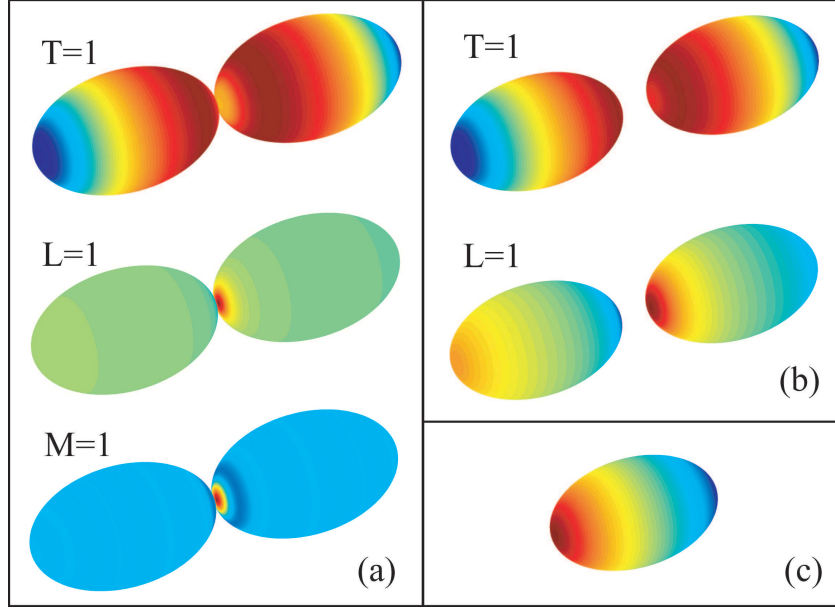


FIG. 3. (Color online) Distribution of a surface charge (a.u.) of the lowest plasmon mode in a cluster of two identical prolate spheroidal nanoparticles according to solution of the equations (14) and (15). The axial-symmetrical case ( $m = 0$ ) is considered, and the aspect ratio of a single spheroid is  $a/c = 0.6$ . The distance between the nanospheroids' centers is  $l/2c = 1.03$  (a),  $l/2c = 1.2$  (b). Distribution of a surface charge in a single spheroid is shown in panel (c). The red color corresponds to the positive charge, and blue - to the negative one.

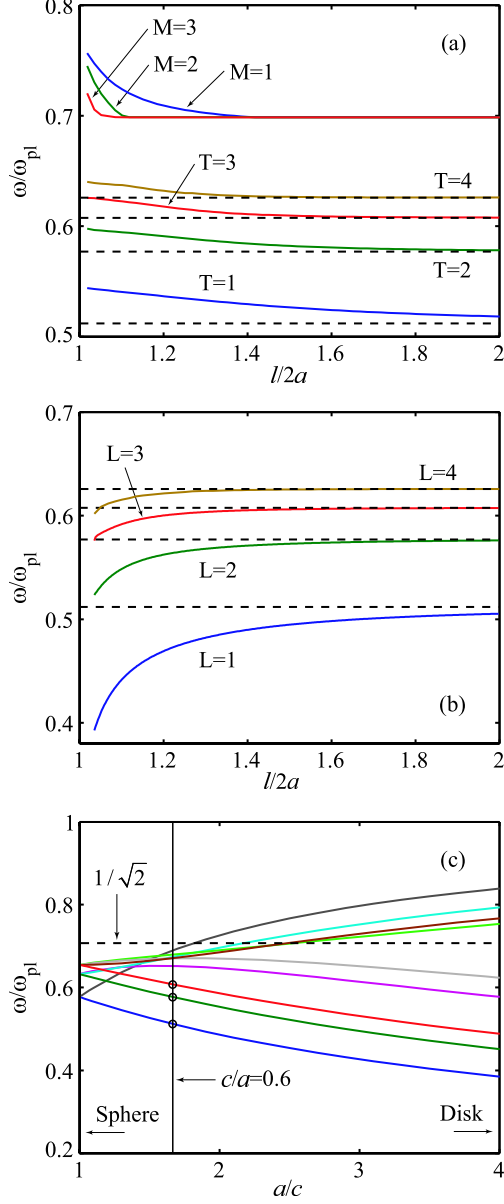


FIG. 4. (Color online) Normalized plasmon frequencies of the first three modes in a cluster of two identical oblate nanospheroids as a function of the distance between their centers. (a) Symmetrical modes (the eigenvalues of Eq. (20)), (b) antisymmetrical modes (the eigenvalues of Eq. (21)). By dashed lines, plasmon frequencies of a single oblate nanospheroid  $\frac{\omega}{\omega_{pl}} = \left\{ \frac{dP_n^m(i\xi_0)}{d\xi_0} Q_n^m(i\xi_0) / \left( \frac{dP_n^m(i\xi_0)}{d\xi_0} Q_n^m(i\xi_0) - P_n^m(i\xi_0) \frac{dQ_n^m(i\xi_0)}{d\xi_0} \right) \right\}^{1/2}$  are shown. The spect ratio of a single oblate nanospheroids is  $c/a = 0.6$  ( $\xi_0 = 1/\sqrt{(a/c)^2 - 1}$ ). The figure (c) shows plasmon frequencies of a single oblate nanospheroid as a function of the inverse aspect ratio  $a/c$ . The vertical line corresponds to  $c/a = 0.6$  and allows to select asymptotic values for the figures (a) and (b).

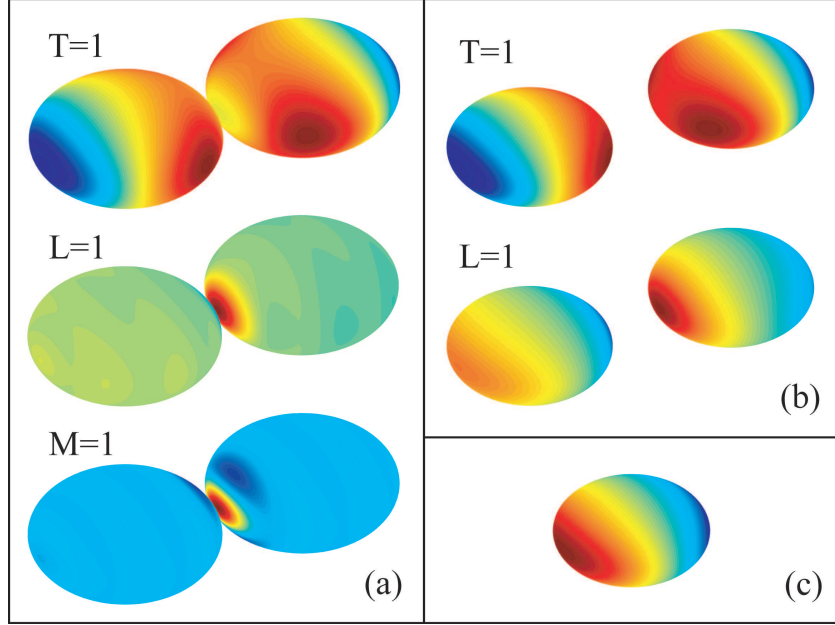


FIG. 5. (Color online) Distribution of a surface charge (a.u.) of the lowest plasmon modes in a cluster of two identical oblate spheroidal nanoparticles according to solution of the equations (20) and (21). The aspect ratio is  $c/a = 0.6$ . The distance between the nanospheroids' centers  $l/2a = 1.05$  (a),  $l/2a = 1.4$  (b). Distribution of a surface charge in a single spheroid is shown in panel (c). The red color corresponds to the positive charge, and blue - to the negative one.

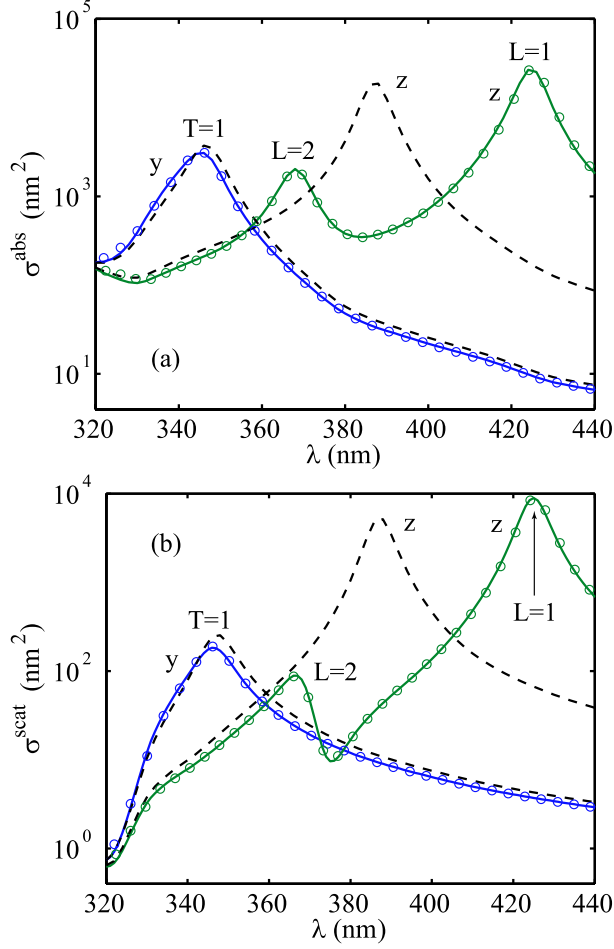


FIG. 6. (Color online) Absorption (a) and scattering (b) cross-sections of a cluster of two identical prolate nanospheroids made from silver as a function of the wavelength. The large semi-axes of the nanospheroids are  $c = 15$  nm, the aspect ratios are  $a/c = 0.6$ , and the distance between the nanospheroids' centers is  $l/2c = 1.05$ . The labels x, y, z correspond to polarization of an incident wave along the x, y, z axis. The circles correspond to finite element simulations with Comsol Multiphysics® software. Doubled absorption cross-section and quadrupled scattering cross-section of a single nanospheroid are shown by dashed curves.

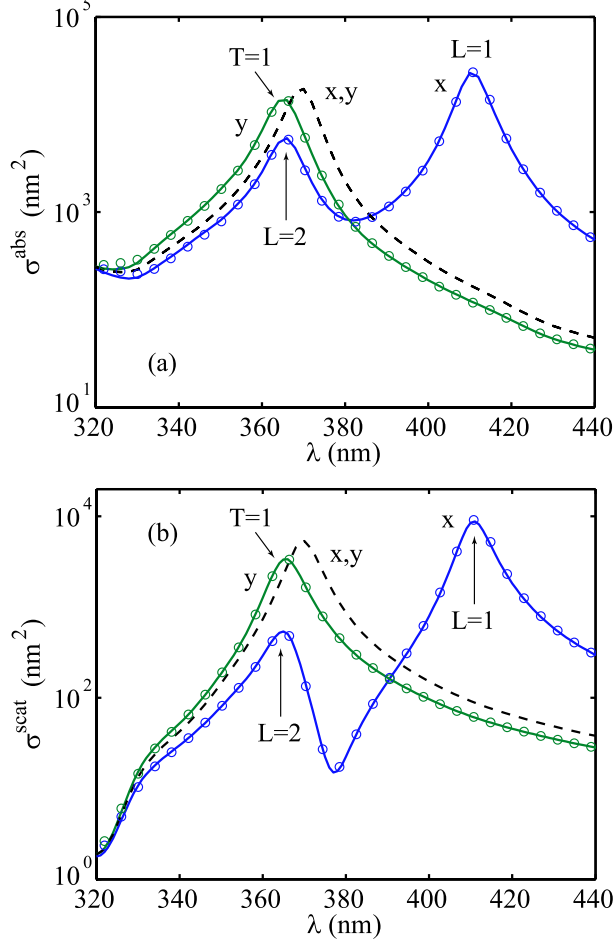


FIG. 7. (Color online) Absorption (a) and scattering (b) cross-sections of a cluster of two identical oblate nanospheroids made from silver as a function of the wavelength. The large semi-axes of the nanospheroids are  $a = 15$  nm, the aspect ratios are  $c/a = 0.6$ , the distance between the nanospheroids' centers is  $l/2a = 1.05$ . The labels x, y, z correspond to polarization of an incident wave along the x, y, z axis. The circles correspond to finite element simulations with Comsol Multiphysics® software. Doubled absorption cross-section and quadrupled scattering cross-section of a single nanospheroid are shown by dashed curves.

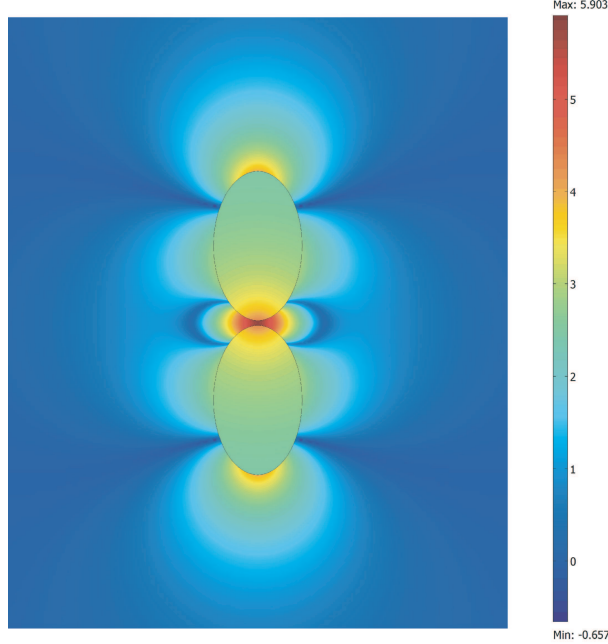


FIG. 8. (Color online) Spatial distribution of  $|\mathbf{E}|^2/|\mathbf{E}_0|^2$  in a cluster of two prolate nanospheroids for  $\lambda = 425$  nm at longitudinal polarization of the excitation field ( $L = 1$  plasmonic resonance, common logarithmic scale).

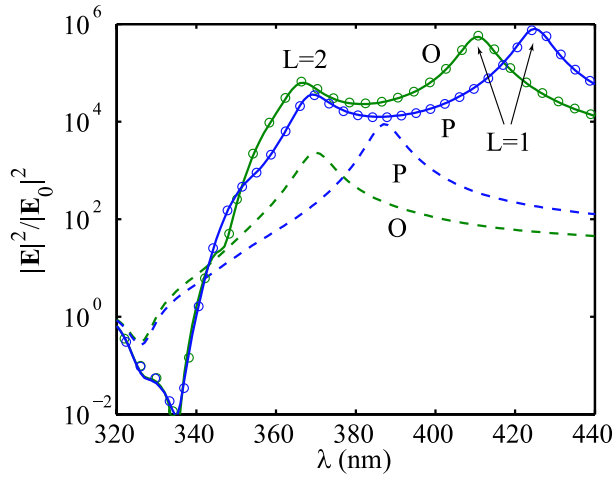


FIG. 9. (Color online) Enhancement of  $|\mathbf{E}|^2$  in the gap between two identical silver nanospheroids as a function of the wavelength. P and O labels correspond to prolate and oblate spheroids correspondingly. The large semi-axes of the nanospheroids are 15 nm, the aspect ratios are 0.6,  $l/2c = 1.05$  for a cluster of prolate spheroids and  $l/2a = 1.05$  for a cluster of oblate spheroids. Enhancements for single nanospheroids are shown by the dashed curve.

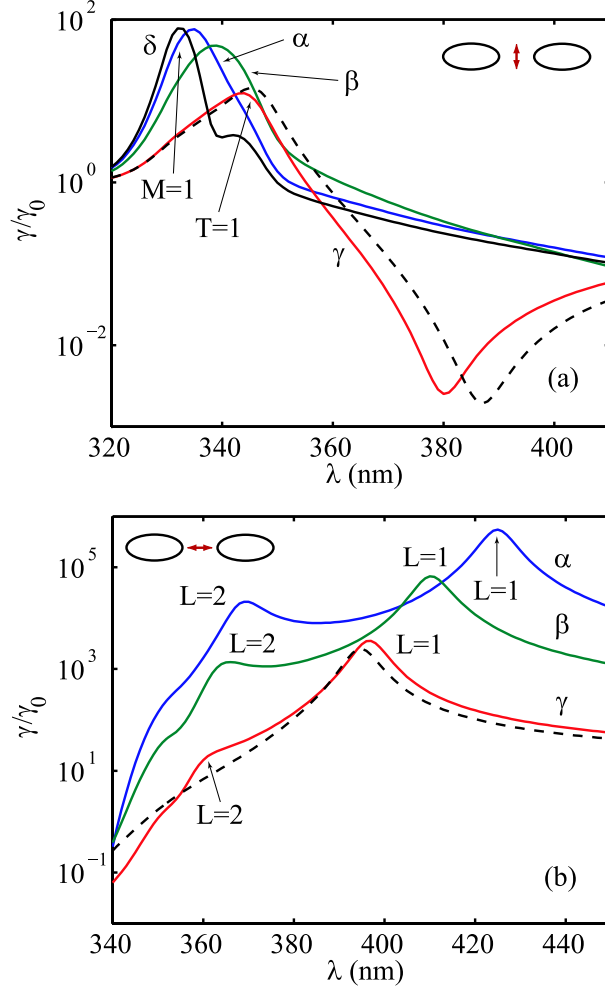


FIG. 10. (Color online) Normalized radiative decay rate of a dipole placed at the middle point between two identical prolate nanospheroids made from silver as a function of the wavelength. The dipole source moment is oriented along the x or y axes (a) and along the z axis (b). The large semi-axes of the nanospheroids are  $c = 15$  nm, the aspect ratios are  $a/c = 0.6$ . The curves  $\alpha$ ,  $\beta$ ,  $\gamma$ ,  $\delta$  correspond to  $l/2c = 1.05$ , 1.1, 1.3 and 1.03, respectively. The asymptotic expression obtained by approximation of the spheroids by point dipoles ( $l/2c = 1.3$ ) is shown by the dashed curve.

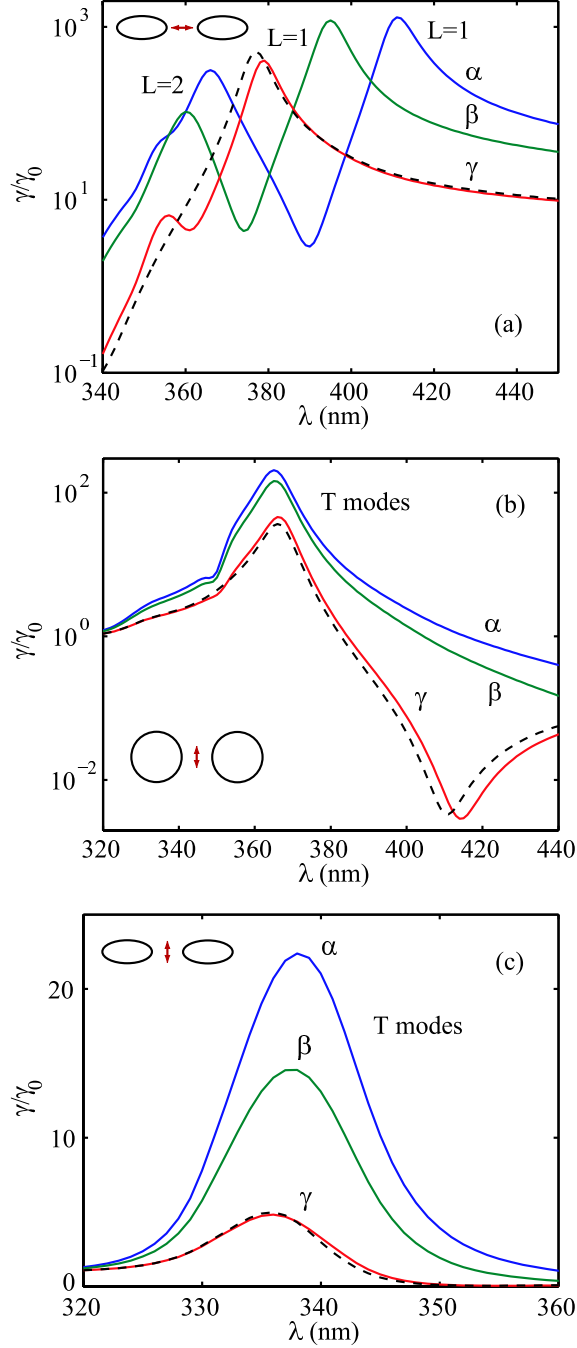


FIG. 11. (Color online) Normalized radiative decay rate of a dipole placed at the middle point between two identical oblate nanospheroids made from silver as a function of the wavelength. The dipole source moment is oriented along the x (a), y (b), and z (c) axis. The large semi-axes of the nanospheroid are  $a = 15$  nm, the aspect ratio is  $c/a = 0.6$ . The curves  $\alpha$ ,  $\beta$ ,  $\gamma$  correspond to  $l/2a = 1.05$ , 1.1, and 1.3, respectively. The asymptotic expression obtained by approximation of the spheroids by point dipoles ( $l/2a = 1.3$ ) is shown by the dashed curve.

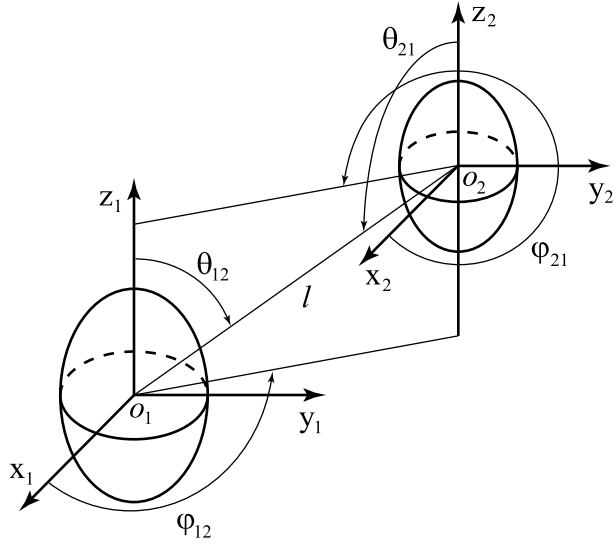


FIG. 12. Geometry of derivation of the translational addition theorem.